

Double-blind test program for astrometric planet detection with Gaia

S. Casertano¹, M. G. Lattanzi², A. Sozzetti^{2,3}, A. Spagna², S. Jancart⁴, R. Morbidelli², R. Pannunzio², D. Pourbaix⁴,
and D. Queloz⁵

¹ Space Telescope Science Institute, 3700 San Martin Drive, Baltimore, MD 21218, USA

² INAF - Osservatorio Astronomico di Torino, via Osservatorio 20, 10025 Pino Torinese, Italy

³ Harvard-Smithsonian Center for Astrophysics, 60 Garden Street, Cambridge, MA 02138, USA

⁴ Institut d'Astronomie et d'Astrophysique, Université Libre de Bruxelles, CP. 226, Boulevard du Triomphe, 1050 Bruxelles, Belgium

⁵ Observatoire de Genève, 51 Ch. de Maillettes, 1290 Sauveny, Switzerland

Received; accepted

ABSTRACT

Aims. The scope of this paper is twofold. First, it describes the simulation scenarios and the results of a large-scale, double-blind test campaign carried out to estimate the potential of Gaia for detecting and measuring planetary systems. The identified capabilities are then put in context by highlighting the unique contribution that the Gaia exoplanet discoveries will be able to bring to the science of extrasolar planets in the next decade.

Methods. We use detailed simulations of the Gaia observations of synthetic planetary systems and develop and utilize independent software codes in double-blind mode to analyze the data, including statistical tools for planet detection and different algorithms for single and multiple Keplerian orbit fitting that use no a priori knowledge of the true orbital parameters of the systems.

Results. 1) Planets with astrometric signatures $\alpha \approx 3$ times the assumed single-measurement error σ_ψ and period $P \leq 5$ yr can be detected reliably and consistently, with a very small number of false positives. 2) At twice the detection limit, uncertainties in orbital parameters and masses are typically 15% – 20%. 3) Over 70% of two-planet systems with well-separated periods in the range $0.2 \leq P \leq 9$ yr, astrometric signal-to-noise ratio $2 \leq \alpha/\sigma_\psi \leq 50$, and eccentricity $e \leq 0.6$ are correctly identified. 4) Favorable orbital configurations (both planets with $P \leq 4$ yr and $\alpha/\sigma_\psi \geq 10$, redundancy over a factor of 2 in the number of observations) have orbital elements measured to better than 10% accuracy > 90% of the time, and the value of the mutual inclination angle i_{rel} determined with uncertainties $\leq 10^\circ$. 5) Finally, nominal uncertainties obtained from the fitting procedures are a good estimate of the actual errors in the orbit reconstruction. Extrapolating from the present-day statistical properties of the exoplanet sample, the results imply that a Gaia with $\sigma_\psi = 8 \mu\text{as}$, in its unbiased and complete magnitude-limited census of planetary systems, will discover and measure several thousands of giant planets out to 3–4 AU from stars within 200 pc, and will characterize hundreds of multiple-planet systems, including meaningful coplanarity tests. Finally, we put Gaia's planet discovery potential into context, identifying several areas of planetary-system science (statistical properties and correlations, comparisons with predictions from theoretical models of formation and evolution, interpretation of direct detections) in which Gaia can be expected, on the basis of our results, to have a relevant impact, when combined with data coming from other ongoing and future planet search programs.

Key words. planetary systems – astrometry – methods: data analysis – methods: numerical – methods: statistical – stars: statistics

1. Introduction

The continuously increasing catalog of extrasolar planets is today surpassing the threshold of 270 planets announced¹. Most of the nearby ($d \lesssim 200 - 300$ pc) exoplanet candidates have been detected around F-G-K-M dwarfs by long-term, high-precision ($1 - 5 \text{ m s}^{-1}$) Doppler search programs (e.g., Butler et al. 2006, and references therein; Udry et al. 2007, and references therein). Over a dozen of these are 'hot Jupiters' with orbital periods $P \approx 1 - 20$ days discovered to cross the disk of their relatively bright ($V < 13$) parent stars thanks to high-cadence, milli-mag photometric measurements². An additional dozen or so extra-

solar planets have been found residing at $d > 300$ pc, thanks to both transit photometry (e.g., Konacki et al. 2003, 2005; Bouchy et al. 2004; Pont et al. 2004, 2007; Udalski et al. 2007; Collier Cameron et al. 2006; Mandushev et al. 2007; Kovács et al. 2007; Bakos et al. 2007) as well as microlensing surveys in the Galactic bulge (e.g., Bond et al. 2004; Udalski et al. 2005; Gould et al. 2006; Beaulieu et al. 2006).

The sample of nearby exoplanets and their host stars is amenable to follow-up studies with a variety of indirect and direct techniques, such as high-resolution (visible-light and infrared) imaging and stellar spectroscopy, and photometric transit timing (for a review, see for example Charbonneau et al. 2007, and references therein). Milli-arcsecond (mas) astrometry for bright planet hosts within 200–300 pc provides precise distance estimates thanks to Hipparcos parallaxes (Perryman et al. 1997). However, despite a few important successes (Benedict et al. 2002, 2006; McArthur et al. 2004; Bean et al. 2007), astrometric measurements with mas precision have so far proved of limited utility when employed as either a follow-up tool or

Send offprint requests to: A. Sozzetti,
e-mail: sozzetti@oato.inaf.it

¹ See, for example, Jean Schneider's Extrasolar Planet Encyclopedia at <http://exoplanet.eu/>

² For a review, see Charbonneau et al. 2007, and references therein. For an updated list, see for example www.unige.ch/pont/TRANSITS.htm, and references therein

to independently search for planetary mass companions orbiting nearby stars (for a review, see for example Sozzetti 2005, and references therein).

In several past exploratory works (Casertano et al. 1996; Casertano & Sozzetti 1999; Lattanzi et al. 1997, 2000a, 2000b, 2002; Sozzetti et al. 2001, 2002, 2003a, 2003b), we have shown in some detail what space-borne astrometric observatories with micro-arcsecond (μas)-level precision, such as Gaia (Perryman et al. 2001) and SIM PlanetQuest (Unwin et al. 2007), can achieve in terms of search, detection and measurement of extrasolar planets of mass ranging from Jupiter-like to Earth-like. In those studies we adopted a qualitatively correct description of the measurements that each mission will carry out, and we estimated detection probabilities and orbital parameters using realistic, non-linear least-square fits to those measurements. For Gaia, we used the then-current scanning law and error model; for SIM, we included reference stars, as well as the target, and adopted realistic observational overheads and signal-to-noise estimates as provided by the SIM Project. Other, more recent studies (Ford & Tremaine 2003; Ford 2004, 2006; Catanzarite et al. 2006) have focused on evaluating the potential of astrometric planet searches with SIM, revisiting and essentially confirming the findings of our previous works.

Although valid and useful, the studies currently available need updating and improving. In the specific case of planet detection and measurement with Gaia, we have thus far largely neglected the difficult problem of selecting adequate starting values for the non-linear fits, using perturbed starting values instead. The study of multiple-planet systems, and in particular the determination of whether the planets are coplanar—within suitable tolerances—is incomplete. The characteristics of Gaia have changed, in some ways substantially, since our last work on the subject (Sozzetti et al. 2003a). Last but not least, in order to render the analysis truly independent from the simulations, these studies should be carried out in double-blind mode.

We present here a substantial program of double-blind tests for planet detection with Gaia (preliminary findings were recently presented by Lattanzi et al. (2005)). The results expected from this study include: a) an improved, more realistic assessment of the detectability and measurability of single and multiple planets under a variety of conditions, parametrized by the sensitivity of Gaia; b) an assessment of the impact of Gaia in critical areas of planet research, in dependence on its expected capabilities; and c) the establishment of several Centers with a high level of readiness for the analysis of Gaia observations relevant to the study of exoplanets.

This paper is arranged as follows. In Section 2 we describe our simulation setup and clearly state the working assumptions adopted (the relaxation of some of which might have a non-negligible impact on Gaia’s planet-hunting capabilities). In Section 3 we present the bulk of the results obtained during our extensive campaign of double-blind tests. Section 4 attempts to put Gaia’s potential for planet detection and measurement in context, by identifying several areas of planetary science in which Gaia can be expected, on the basis of our results, to have a dominant impact, and by delineating a small number of recommended research programs that can be conducted successfully by the mission as planned. In section 5 we summarize our findings and provide concluding remarks.

2. Protocol definition and simulation setup

2.1. Double-blind tests protocol

For the purpose of this study, we have devised a specific protocol for the double-blind tests campaign. Initially, three groups of participants are identified: 1) the *Simulators* define and generate the simulated observations, assuming specific characteristics of the Gaia satellite; simulators also define the type of results that are expected for each set of simulations; 2) the *Solvers* receive the simulated data and produce “solutions”—as defined by the simulators; solvers define the criteria they adopt in answering the questions posed by the simulators; 3) the *Evaluators* receive both the “truth”—i.e., the input parameters—from the simulators and the solutions from the solvers, compare the two, and draw a set of conclusions on the process.

A sequence of tasks, each with well-defined goals and time scales, has been established. Each task requires a separate set of simulations, and is carried out in several steps:

1. **Simulation:** The Simulators make the required set of simulations available to the Solvers, together with a clear definition of the required solutions.
2. **Clarification:** A short period after the simulations are made available in which the Solvers request any necessary clarification on the simulations themselves and on the required solutions; after the clarification period, there is no contact between Simulators and Solvers until the Discussion step.
3. **Delivery:** On a specified deadline, the Simulators deliver the input parameters for the simulations to the Evaluator, and the Solvers deliver their solutions together with a clear explanation of the criteria they used—e.g., the statistical meaning of “detection”, or how uncertainties on estimated parameters were defined.
4. **Evaluation:** The Evaluators compare input parameters and solutions and carry out any statistical tests they find useful, both to establish the quality of the solutions and to interpret their results in terms of the capabilities of Gaia, if applicable.
5. **Discussion:** The Evaluators publicize their initial results. All participants are given access to input parameters and all solutions, and the Evaluators’ results are discussed and modified as needed.

2.2. Observing scenario

The simulations were provided by the group at the Torino Observatory. The simulations were made available via WWW as plain text files. A detailed description of the code for the simulation of Gaia astrometric observations can be found in our previous exploratory works (Lattanzi et al. 2000a; Sozzetti et al. 2001). We summarize here its main features.

Each simulation consists of a time series of observations (with a nominal mission lifetime set to 5 years) of a sample of stars with given (catalog) low-accuracy astrometric parameters (positions, proper motions, and parallax). Each observation consists of a one-dimensional coordinate in the along-scan direction of the instantaneous great circle followed by Gaia at that instant. The initially unperturbed photocenter position of a star is computed on the basis of its five astrometric parameters, which are drawn from simple distributions, not resembling any specific galaxy model. The distribution of two-dimensional positions is random, uniform. The distribution of proper motions is Gaussian, with dispersion equal to a value of transverse velocity $V_T = 15 \text{ km sec}^{-1}$, typical of the solar neighborhood. The photocenter position can then be corrected for the gravitational

perturbation of one or more planetary mass companions. The Keplerian motion of each orbiting planet is described via the full set of seven orbital elements. For simplicity, all experiments described here were produced assuming stellar mass $M_\star = 1 M_\odot$. The resulting astrometric signature (in arcsec) is then expressed as $\alpha = (M_p/M_\star) \times (a_p/d)$, where M_p is the planet mass, a_p is the planet orbital semi-major axis and d is the distance to the system (in units of M_\odot , AU, and pc, respectively). Simulated observations are generated by adding the appropriate astrometric noise, as described in the next section.

Finally, the Gaia scanning law has been updated to the most recent expectations (precession angle around the Sun direction $\xi = 50^\circ$, precession speed of the satellite's spin axis $v_p = 5.22 \text{ rev yr}^{-1}$, spin axis rotation speed $v_r = 60 \text{ arcsec s}^{-1}$), which result in fewer observations and possibly less ability to disentangle near-degenerate solutions than with the original scanning law (e.g., Lindegren & de Bruijne 2005). Each star is observed on average $N_{\text{obs}} = 43$ times³; note that the simplest star+planet solution has 12 parameters, and therefore the redundancy of the information is not very high.

2.3. Assumptions and caveats

The simulated data described above indicate that a number of working assumptions have been made. In particular, a variety of physical effects that can affect stellar positions have not been included, and a number of instrumental as well as astrophysical noise sources have not been considered (for a detailed review, see for example Sozzetti 2005). Our main simplifying assumptions are summarized below.

- 1) the position of a star at a given time is described in Euclidean space. A general relativistic formulation of Gaia-like global astrometric observations, which has been the subject of several studies in the recent past (Klioner & Kopeikin 1992; de Felice et al. 1998, 2001, 2004; Vecchiato et al. 2003; Klioner 2003, 2004), has not been taken into account;
- 2) we assume that the reconstruction and calibration of individual great circles have been carried out, with nominal zero errors (i.e., knowledge of the spacecraft attitude is assumed perfect). We refer the reader to e.g. Sozzetti (2005), and references therein, for a summary of issues related to the complex problem of accurately calibrating out attitude errors (due to, e.g., particle radiation, thermal drifts, and spacecraft jitter) in space-borne astrometric measurements;
- 3) the abscissa is only affected by random errors, and no systematic effects are considered (e.g., zero-point errors, chromaticity, radiation damage, etc...). A simple Gaussian measurement error model is implemented, with standard deviation $\sigma_\psi = 8 \mu\text{as}$, which applies to bright targets ($V < 13$). In this context, the projected end-of-mission accuracy on astrometric parameters is $4 \mu\text{as}$. Recently, Gaia has successfully passed the Preliminary Design Review and entered phase C/D of the mission development. ESA has selected EADS-Astrium as Prime Contractor for the realization of the satellite. Scanning law and astrometric section of the selected payload, the only of relevance here, remain largely consistent with the assumptions adopted in our simulations. However, very recent estimates of the error budget indicate a possible

degradation of 35% – 40% (i.e., $\sim 11 \mu\text{as}$) in the single-measurement precision, corresponding to a typical final accuracy of 5 – 5.5 μas for objects in the above magnitude range, with some dependence on spectral type (red objects performing closer to specifications). We will address in the discussion section the possible impact of such performance degradation on Gaia's planet-hunting capabilities;

- 4) light aberration, light deflection, and other apparent effects (e.g., perspective acceleration) are considered as perfectly removed from the observed along-scan measurements;
- 5) when multi-component systems are generated around a target, the resulting astrometric signal is the superposition of two strictly non-interacting Keplerian orbits. It is recognized that gravitational interactions among planets can result in significant deviations from purely Keplerian motion (such as the case of the GJ 876 planetary system, e.g. Laughlin et al. 2005). However, most of the multiple-planet systems discovered to-date by radial-velocity techniques can be well modeled by planets on independent Keplerian orbits, at least for time-scales comparable to Gaia's expected mission duration;
- 6) a number of potentially important sources of 'astrophysical' noise, due to the environment or intrinsic to the target, have not been included in the simulations. In particular, we have not considered a) the dynamical effect induced by long-period stellar companions to the targets, b) the possible shifts in the stellar photocenter due to the presence of circumstellar disks with embedded planets (Rice et al. 2003a; Takeuchi et al. 2005), and c) variations in the apparent stellar position produced by surface temperature inhomogeneities, such as spots and flares (e.g. Sozzetti 2005, and references therein; Eriksson & Lindegren 2007).

The geometric model of the measurement process is described in detail in the Appendix.

3. Results

The double-blind test campaign encompassed a set of experiments that were necessary to establish a reliable estimate of the planet search and measurement capabilities of Gaia under realistic analysis procedures, albeit in the presence of an idealized measurement process. In particular, a number of different tasks were designed, such that the participating groups would be able a) to analyze data produced by a nominal satellite, without taking into account the imperfections due to measurement biases, non-Gaussian error distributions, imperfections in the sphere solution, and so on; b) to convert any Gaussian error model for Gaia measurements into expected detection probability—including completeness and false positives—and accuracy in orbital parameters that can be achieved within the mission; c) to assess to what extent, and with what reliability, coplanarity of multiple planets can be determined, and how the presence of a planet can degrade the orbital solution for another.

We broke down the work plan into three tests: T1, T2, and T3, whose main results are presented below. To facilitate reading, we have chosen to provide the summaries of the results concerning each of the three tests at the beginning of the corresponding sub-sections.

3.1. Test T1: Planet detection

Test T1 is designed primarily to establish the reliability and completeness of planet detections for single-planet systems based on simulated data, with full *a priori* understanding of their noise

³ We define as elementary observation the successive crossing of the two fields-of-view of the satellite, separated by the basic angle $\gamma = 106.5^\circ$.

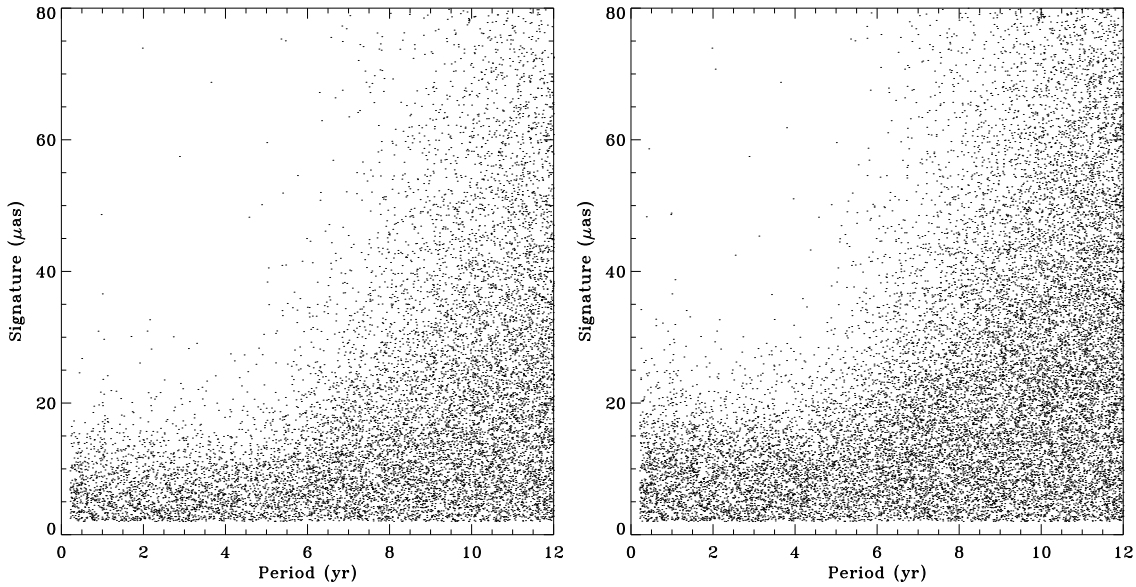


Fig. 1. Left: Distribution of period and signature for the planets missed by Solver A's broad criterion (A1). If more than one planet is present, the one with the largest signature is plotted. Right: distribution of period and signature for the planets missed by criterion B1.

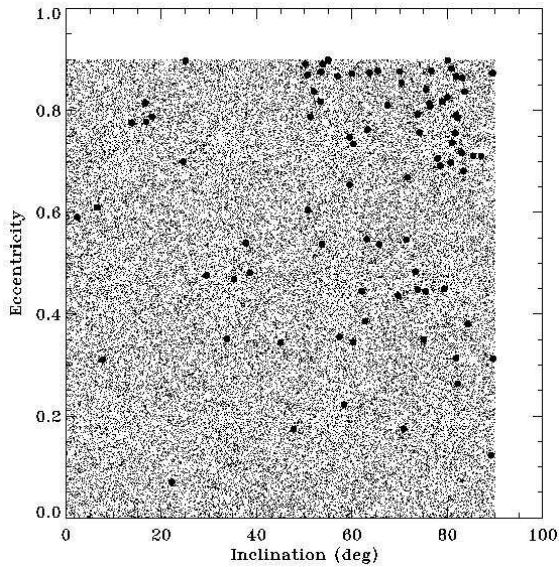


Fig. 2. Inclination and eccentricity of the planets simulated for the T1 experiment. Black dots are planets with $\alpha < 15 \mu\text{as}$ and $P < 6 \text{ yr}$ not detected by the A1 criterion.

characteristics. Simulated data were prepared for 100,000 stars. Of these, 45,202 have no planets, 49,870 one, 3878 two, and 1050 have three planets. The astrometric signature of each planet ranges from 0.8 to $80 \mu\text{as}$ ($0.1 \leq \alpha/\sigma_\psi \leq 10$), the period P from 0.2 to 12 years, while eccentricities are drawn from a random distribution within the range $0.0 \leq e \leq 0.9$. All other orbital elements (inclination i , longitude of pericenter ω , pericenter epoch τ , and position angle of the nodes Ω) were distributed randomly as follows: $1^\circ \leq i \leq 90^\circ$, $0^\circ \leq \omega \leq 360^\circ$, $0 \leq \tau \leq P$, and $0^\circ \leq \Omega \leq 180^\circ$. For systems with multiple planets, there was no specific relationship between periods, phases, or amplitudes of the planetary signatures. The distribution of planetary signatures was unknown to the solvers.

On this dataset, solvers were asked to carry out two tests. Test T1 consisted of identifying the likely planet detections, based on a single-star analysis and criteria of the Solvers' own choosing. Test T1b gave the opportunity to the solvers to improve on their planet detection on the basis of an orbital fit, i.e., using the knowledge that the deviations from a single-star model were in fact expected to have the signature of a star-planet system. Two Solvers participated in this step and provided completely independent solutions. Solver A attempted to improve the quality of planet detection using orbital fits, in the spirit of the T1b test; Solver B was satisfied with the quality of the detection achieved from the statistical properties of the residuals to the single-star fit. Although the solvers used different detection criteria and post-processing analysis, both ultimately achieved good (and comparable) detection quality, indicating that the procedures they used are robust and consistent. In particular, the T1 experiment has shown that, at least for the cases under consideration, detection tests (e.g., χ^2 or $F2$) based on deviations from the single-star astrometric solution perform as well as can be expected. Planets down to astrometric signature $\alpha \simeq 2\sigma_\psi$ can be detected reliably and consistently, with a very small number of false positives. Even better, the choice of the detection threshold is an effective way to distinguish between highly reliable and marginal candidates. Under the assumptions of this test, which is based on an idealized, perfectly known noise model, potential planet-bearing stars can be identified and screened reliably. Refinements of the detection criteria based on additional considerations, e.g., the quality of the orbital fit, can potentially make an improvement in the fitting procedure. However, the performance of a straight χ^2 or $F2$ test is already extremely good; such tests, if properly applied, can yield candidates with the expected range of sensitivity and with a powerful discrimination against false positives.

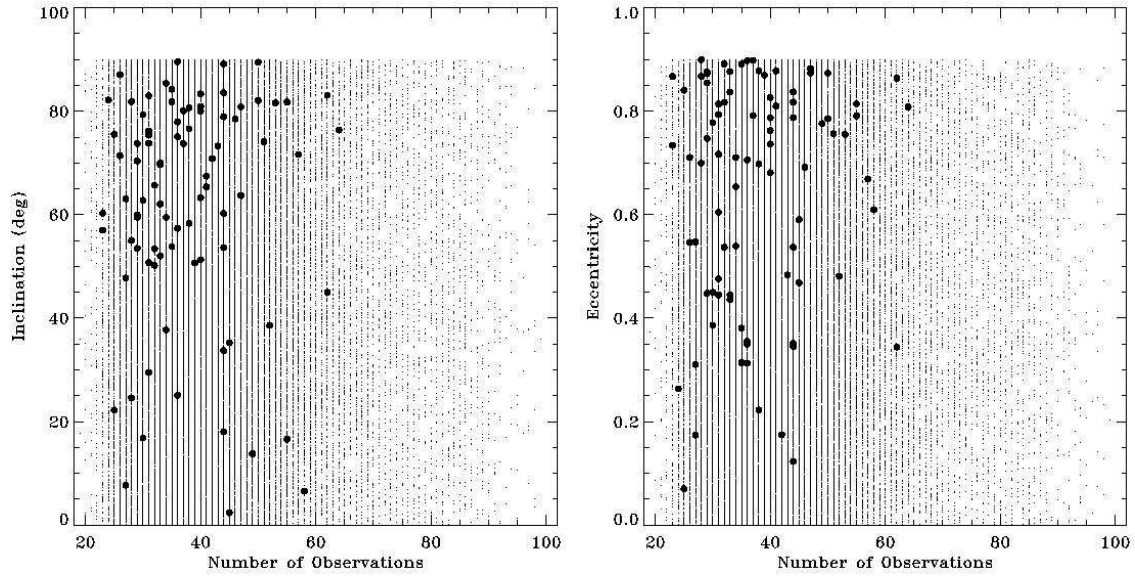


Fig. 3. Left: same as Figure 2, but here the results are expressed in terms of inclination angle and number of observations. Right: same as Figure 2, in the e - N_{obs} plane.

3.1.1. First-pass detection

Both solvers approach test T1 on the basis of the quality of the single-star, five-parameter solution for the astrometric measurements.

Solver A adopts two criteria to identify candidate planets, one broad, aimed at detecting as many candidates as reasonable, and one strict, designed to reduce the number of false positives. Specifically, Solver A uses $P(\chi^2)$, the probability that the observed χ^2 of the single-star solution is as bad or worse than the value observed in the presence of pure measurement errors, and $P(F)$, the F-test probability on the same fit. A large value of χ^2 or of the F statistic can readily arise if the deviations due to the presence of a planet are much larger than the expected measurement errors, and thus a low value of $P(\chi^2)$ and $P(F)$ signifies likely planet (and unlikely false positive).

The broad criterion, A1, requires only that $P(\chi^2) < 0.05$, and favors completeness over reliability: many more marginal candidates are included, but false positives will be more numerous. The strict criterion, A2, requires both $P(\chi^2) < 0.0001$ and $P(F) < 0.0001$, and favors reliability over completeness: candidates satisfying this criterion have a small probability of being false positives, but many marginal cases will be missed.

Criterion A1 identifies 44,914 candidates, of which 42,810 are indeed planets and 2,104 are false positives, close to the 5% expected from the criterion. On the other hand, 11,988 planets are missed by this criterion. Typically, the planets missed have signature smaller than $15 \mu\text{as}$ or period longer than 5 years (Figure 1, left panel), high eccentricity and/or close to edge-on orbits (Figure 2), and relatively small numbers of observations ($N_{\text{obs}} < 40$, Figure 3). The performance of this and other criteria discussed here is summarized in Table 1.

Criterion A2 yields only 28,655 detections, with *no* false positives, but misses 26,143 planets—only half of the true planets are found. Because of the more demanding criteria, planets with signature up to $30 \mu\text{as}$ can be missed by this criterion, regardless of period. Nonetheless, the dramatic drop in false positives is very important, and would probably favor the stricter criterion.

A further refinement of Solver A's search criterion is discussed below. However, it is worth noting that a criterion based purely on $P(\chi^2) < 0.0001$, without the $P(F)$ requirement, would detect 34,918 planets, only 4 of which are false positives, and miss 19,880—a substantially better performance at the cost of a modest number of false positives.

Solver B adopts a similar method, using specifically the $F2$ indicator (see the Hipparcos Catalogue, vol. 1, p. 112), which is expected to follow a normal distribution with mean 0 and dispersion 1. His criterion, B1, requires $|F2| > 3$, which in essence is a 3-sigma criterion. With this criterion, Solver B identifies 37,643 correctly as having a planet (or more), while 17,155 are missed and 106 (0.2% of the no-star sample) are false positives. Similarly to A1, the missed planets mostly have signature smaller than $20 \mu\text{as}$ or period longer than 5 years (Figure 1, right panel). The overall distribution is similar to that of planets missed by A1, although more marginal cases are excluded—and fewer false positives are included.

Criterion B1 appears to be preferable to A1, which finds 5,000 more planets at the cost of nearly 2,000 false positives. If a 0.2% incidence of false positives is considered acceptable, the performance is also better than that of A2, with nearly 9,000 more planets found at a modest cost in false positives. However, the simple $P(\chi^2) < 0.0001$ criterion finds nearly as many planets, with a much smaller fraction of false positives. In practice, the choice between these criteria would depend on the specific application and sample properties. For example, for the simulated data studied here, a fine-tuned $P(\chi^2)$ test, e.g., with threshold set at 0.001 (C1), would find 37,714 valid candidates (about as many as B1 and 2,000 fewer than A4, discussed below) and only 68 false positives.

3.1.2. Refining the detection criteria

Realizing that his strict criterion (which requires both $P(\chi^2) < 0.0001$ and $P(F) < 0.0001$) may be too stringent, while the simple $P(\chi^2) < 0.05$ criterion is expected to allow too many false positives, Solver A attempts a detection refinement based on the quality of the orbital fit, in the spirit of the T1b test.

Table 1. Summary of detection probability

Name	Criterion	Detections			Missed
		Total	True	False	
A1	$P(\chi^2) < 0.05$	44 914	42 810	2 104	11 988
A2	$P(\chi^2) < 0.0001, P(F) < 0.0001$	28 655	28 655	0	26 143
A3	$P(\chi^2) < 0.0001$ or $P(\chi^2) < 0.05, P(\chi^2)_{\text{orbital}} > 0.2$	40 196	39 630	566	15 168
A4	$P(\chi^2) < 0.0001$ or $P(\chi^2) < 0.05, P(\Delta\chi^2) < 0.001$	39 957	39 768	189	15 030
B1	$ F2 > 3$	37 749	37 643	106	17 155
C1	$P(\chi^2) < 0.001$	37 782	37 714	68	17 084

For the purpose of this test, Solver A considers the “marginal” candidates with $0.0001 < P(\chi^2) < 0.05$; of these, 2,100 are in fact false positives, while 7,892 have a real planet. In this case, there are 34,918 non-marginal detections—those with $P(\chi^2) < 0.0001$ —of which only 4 are false detections.

The first refinement (A3) is based on the quality of the orbital fit: a marginal candidate passes if the χ^2 statistics of the residuals after the orbital fit improves to $P(\chi^2) > 0.2$ (a minimum factor 4 improvement). A total of 5,274 marginal candidates pass this test; of these, 11% are false detections. Of the marginal candidates that do not pass the refinement, 33% are false positives. Thus, this orbital refinement does improve the probability that the candidate is real, and can in fact increase the sample of possible candidates (see Table 1).

The second refinement for the marginal candidates (A4) is based on the likelihood ratio test applied to the two fits, with or without the planet. For a candidate to pass, the fit with the planet is required to improve the χ^2 with a probability better than 0.001, i.e., $P(\Delta\chi^2) < 0.001$. Of the 5,035 stars that pass, 96% do in fact have a planet; only 185 are false positives. The likelihood ratio improvement appears to perform significantly better than the simpler test based on the new χ^2 probability (see Table 1).

The refined criteria, especially A4, do improve substantially on A1, bringing its performance in line with that of B1. A4 finds about 2,000 more candidates than B1, but 83 more false positives. B1 is simpler to apply, and the expected distribution of the $F2$ statistic is well-defined in the case of stars without planets; this makes it possible to clearly label those candidates that are most likely to be false positives, and therefore to derive samples with different levels of confidence for different purposes. On the other hand, A4 offers the potential to detect more stars, including potentially some stars with relatively small signatures but a good orbital fit, without an excessive increase in the number of false positives. Neither approach offers the freedom from false detections of A2, which however comes at the cost of fewer candidates.

It may be worthwhile considering orbital fit criteria as a means to improve the detection statistics for a more tightly selected initial sample. For example, one could consider a likelihood ratio threshold that depends on the original $P(\chi^2)$, so that more marginal candidates (with a greater probability of being false positives) are held to a stricter likelihood ratio requirement. Conceivably, such requirements could achieve a better combination of sensitivity and reliability than straight χ^2 or $F2$ tests. However, their investigation is beyond the scope of this analysis; a new set of tests would be needed to assess such techniques in true double-blind fashion.

3.2. Test T2: Single-planet orbit determination

The T2 experiment is designed primarily to establish the accuracy of the orbital determination for single planets with solidly detected signatures, under the assumption that the noise characteristics of the data are fully understood. Solvers knew that each star had one planet, but did not know the distribution of signatures and periods. The T2 test determines how well the orbital parameters of a single planet can be measured for a variety of signature significance, period, inclination, and other parameters. Simulated data were prepared for 50,000 stars, each with exactly one planet with signatures ranging between $16 \mu\text{as}$ (astrometric signal-to-noise $\alpha/\sigma_\psi = 2$) and 1.6 mas ($\alpha/\sigma_\psi = 200$) and periods between 0.2 and 12 years; all other orbital parameters were randomly distributed with the same prescriptions of Test T1.

Each solver was asked to carry out a full orbital reconstruction analysis for each star, beginning from the period search and including error estimates for each of the orbital parameters. As for the T1 test, two solvers, A and B, participated in this test, each with their independently developed numerical code. The first, obvious conclusion is that both solvers achieve very good results, recovering very solidly the orbital parameters of the vast majority of ‘good’ cases - those with high astrometric signature and period shorter than the mission duration. In addition, their results are extremely consistent, indicating the robustness of the procedures they developed and of the overall approach.

Both Solvers run their respective pipelines, consisting of detection, initial parameter determination, and orbital reconstruction, on each of the 50,000 simulated time series provided by the Simulators. They have no a priori knowledge of the orbital properties of each planet, although they do know that each star is expected to have one and only one planet.

In both cases, solvers use the equivalent of a least-squares algorithm to fit the astrometric data for each planet; they need to solve for the star’s basic astrometric information (position, parallax, proper motion), for which only low-accuracy catalog parameters are provided, as well as for the parameters of the reflex motion. Solver B provides orbital solutions expressed in terms of P, e, τ , and the four Thiele-Innes parameters A, B, F, G (e.g., Green 1985). He provides also estimated uncertainties for each parameter and the full covariance matrix. Solver A also provides P, e , and τ , but instead of the Thiele-Innes parameters, he returns a, i, Ω , and ω . He computes formal errors for each parameter, but not the covariance matrix.

Solver B reports no solution for 521 stars, about 1% of the total. Solver A reports a solution for all stars, but 69 are invalid as the estimated error in the orbital parameters is undefined; we exclude these objects from further consideration. In addition, a few tens of objects have very large errors, and may not be meaningful. It is important to note that for both solvers the number of such cases is very small, and—as they are identified during

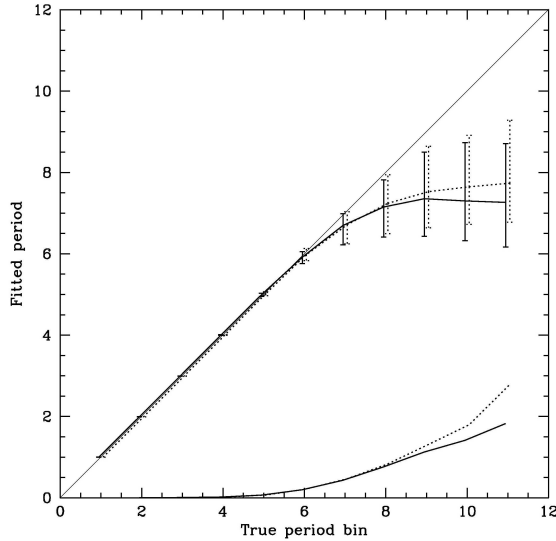


Fig. 6. Distribution of estimated periods and their errors for orbits with signature larger than 0.4 mas as a function of true period. The lines with error bars show the median and interquartile range for the period estimated by Solver A (solid) and B (dashed). The lines without error bars represent the median estimated errors from the fitting procedure for Solver A (solid) and B (dashed).

the solution process—they present no risk of contaminating the search for planets; they simply reflect the limitations of the observations.

3.2.1. Retrieving orbital parameters

The orbital period is perhaps the most important of the orbital parameters, and generally the most critical in terms of obtaining an orbital solution that is close to the truth. Period search is usually a delicate process, and aliasing, especially for relatively sparsely sampled orbits, can be a serious concern. Therefore the evaluation of the solutions starts with the orbital period. In summary, the period is retrieved with very good accuracy and small bias for true periods ranging from 0.3 to 6 years. A small fraction of very short and very long periods are aliased to very different periods; these cannot be readily identified by simply inspecting the estimated errors. Long periods are systematically underestimated; this trend is predictable on the basis of simulations, and the amount of bias is comparable to the estimated period error.

Figure 4 shows the quality of the match between the true period and the solution by Solver B (Solution 1) and by Solver A (Solution 2). For the 20,411 stars with true period shorter than 5 years, both solvers recover over 98% with a fractional error in the period of 10% or smaller (20,054 for Solver A, 20,158 for Solver B). This includes a few cases (45 for Solver A, 27 for Solver B) for which no valid solution is returned. Almost all the cases with poor period determination have either very small signatures or periods shorter than 3 months, for which aliasing can occur with the relatively sparse sampling of the Gaia scanning law. Such cases are rare, no more than 2% of all short-period planets, but are not readily identified by the nominal error in the period. Short-period solutions will probably need to be looked at more carefully to eliminate the possibility of aliasing in the solution.

While fidelity is extremely good for planets with true period ranging from a few months to the mission lifetime, the quality

of the solution degrades quickly for periods longer than the mission duration. Visually, it is clear that - for given amplitude of the perturbation - the ability to recover the planet's period with modest errors starts degrading at periods of about 6 years. Note also that for very long true periods, the fitted period is systematically shorter than the truth; at 10 years, the typical recovered period is substantially shorter, about 7 years, with a very large dispersion. In a small number of cases (418 for Solver A, 150 for Solver B), a very small period is fitted to a long period object (resulting in the small cloud of points near the $P = 0$ axis in both panels of Figure 4), indicating that the fit has aliased into a completely different range.

Figure 5 shows the error in the period, as estimated by each Solver, as a function of true period. As in the period difference, the estimated error also increases greatly with increasing period, and in fact the estimated uncertainties are comparable with the error in the fitted period shown in Figure 4.

The comparison between error in fitted period and estimated error is shown in a more quantitative way in Figure 6. The curves and error bars illustrate the median and quartiles of the fitted period distribution in bins of true period, solid for Solver A and dotted for Solver B; the thin diagonal dashed line corresponds to exact solutions. As it can be clearly seen, the period solution is very good, without indication of significant bias, up to about 6 years, beyond which the solution underestimates the period. The median estimated errors (lower curves) match the interquartile range reasonably well.

Figure 7 shows how the period accuracy varies with signature for periods around 1, 3, 5, and 6 years. In each case, larger signatures mean a stronger astrometric signal, and thus better accuracy; the distribution of errors matches well the estimate from the solution itself. In each panel, the blue dots (scale to the left) represent the difference between fitted and true period as function of true signature in the stated period range, and the red dots (scale to the right) show the error as estimated by the solver for that particular orbit. The solid lines and points represent the median values for a 0.2 mas bin in signature; the error bars for the period error show the range between the first and third quartile in each bin. Panels to the left refer to solutions by Solver A, to the right by Solver B. In each panel and for each signature bin, the median estimated error (red triangles) is very close to the difference between median and quartile error for the same set of solutions, indicating that the estimated errors are a good guide to the true errors. The median of the difference between fitted and true period (blue squares) is generally small, showing that there is very little bias in the period estimate.

The other orbital parameters are similarly well estimated for the vast majority of "good" orbital solutions, excluding those with low signature and long period. For example, Figure 8 compares the eccentricity fitted by the two Solvers with the true value for all stars with period shorter than 5 years and signature larger than 0.4 mas, which corresponds to the top 75% in signature. Similarly, Figure 9 shows the true and fitted (by Solver B) values of the Thiele-Innes parameters A and B for the same cases. Clearly both sets of parameters represent high quality orbital fits. Other orbital parameters follow similar patterns.

Finally, it is worth mentioning how subtle differences in the orbital solutions carried out by the two solvers can be seen if one focuses on regimes of relatively low astrometric signal. We show for example in Figure 10 the comparison between the distributions of fitted P and e for Solver A and Solver B in cases of $5 < \alpha/\sigma_\psi < 10$ and $3 < \alpha/\sigma_\psi < 5$, and restricting ourselves to good solutions for which P is within 10% of the true value and e differs from the true value by no more than 0.1. On the one

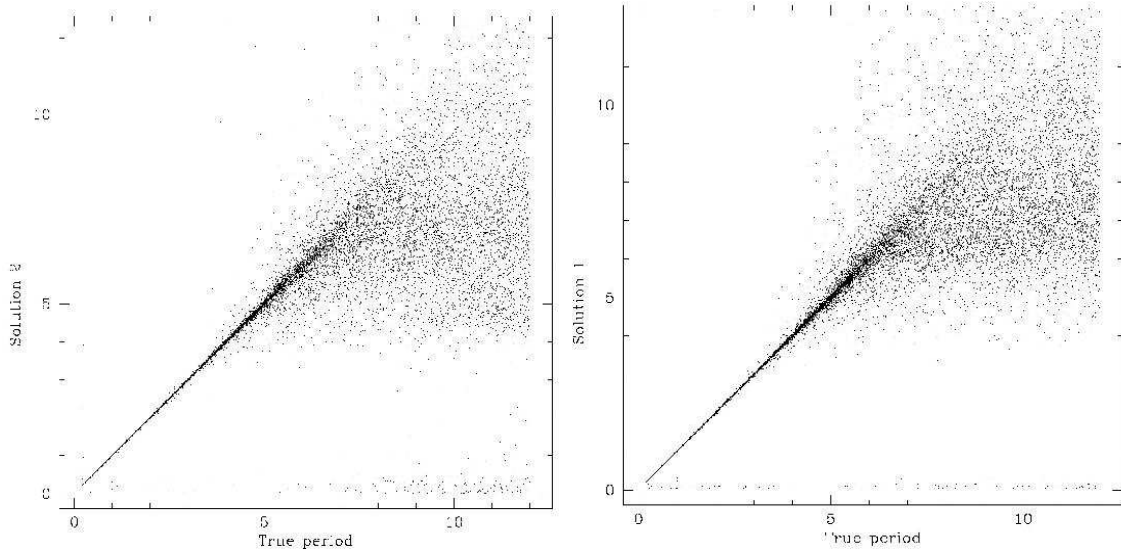


Fig. 4. Distribution of fitted period as a function of true period for Solver A (left) and B (right).

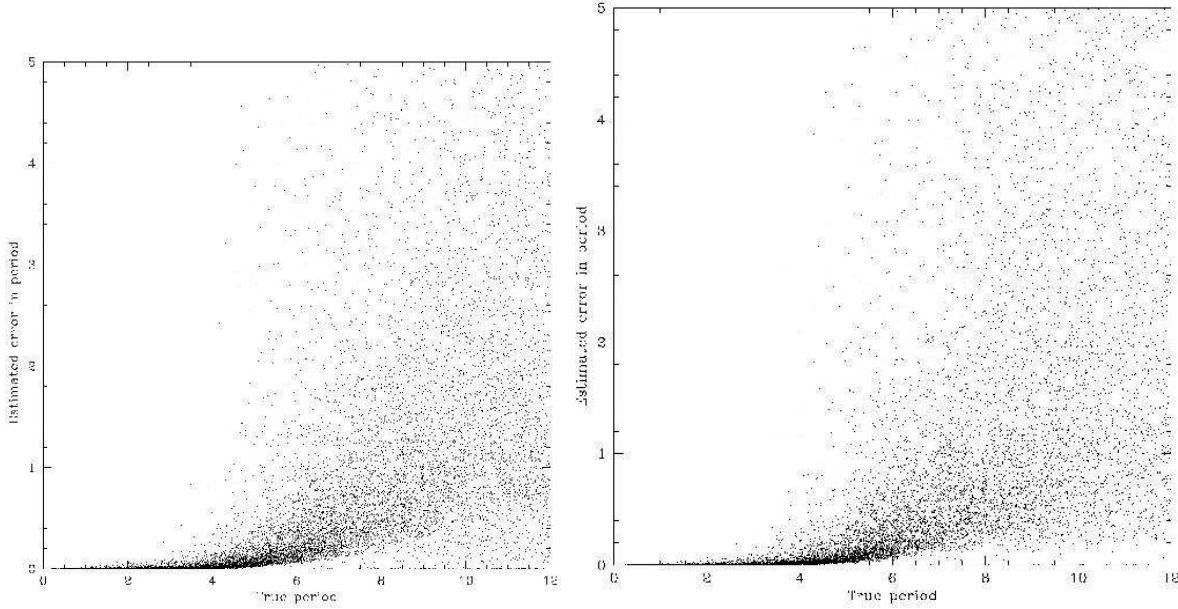


Fig. 5. Distribution of estimated error in the period as a function of true period for Solver A (left) and B (right).

hand, from the Figure it is clear how both solvers identify and measure precisely orbital periods for virtually the same stars; a Kolmogorov-Smirnov (K-S) test gives a probability that the two distributions are the same of 0.15 and 0.98 for the two regimes of signal strength investigated. On the other hand, the distributions of well-measured eccentricities are significantly different, with a the K-S test giving a probability of the null hypothesis of 0.04 and 0.005, respectively. The most obvious feature is the increase in the number of very large eccentricity values ($e \geq 0.6$) correctly identified by Solver A with respect to Solver B. In particular, in the range $3 < \alpha/\sigma_\psi < 5$ Solver A measures accurately the eccentricity for some 23% more stars than Solver B. A possible explanation for this discrepancy maybe found in the different approaches the two solvers adopt to reach the configuration of initial starting guesses for the parameters in the orbital fits. Both solvers tackle this issue implementing a two-tiered strategy consisting of a combined global+local minimiza-

tion procedure. Solver A uses a methodology similar to that described in Konacki et al. (2002), in which a Fourier expansion of the Keplerian motion is used to derive initial guesses of the full set of orbital elements, subsequently utilized in a local non-linear least-squares analysis. Instead, Solver B adopts a scheme in which a guess to P is obtained using a period-search technique (e.g. Horne & Baliunas 1986), and then an exploration of the (e, τ) -space is carried out to derive the linear parameters A , B , F , and G as the unique minimizer of χ^2 when e , P , and τ are fixed (e.g., Pourbaix 2002). However, for highly non-linear fitting procedures with a large number of model parameters the statistical properties of the solutions are not at all trivial (and significantly differ from those of linear models). A serious study of differences in the fitting procedures adopted by the two Solvers would require, for example, an in-depth analysis of the relative agreement between a variety of statistical indicators of the qual-

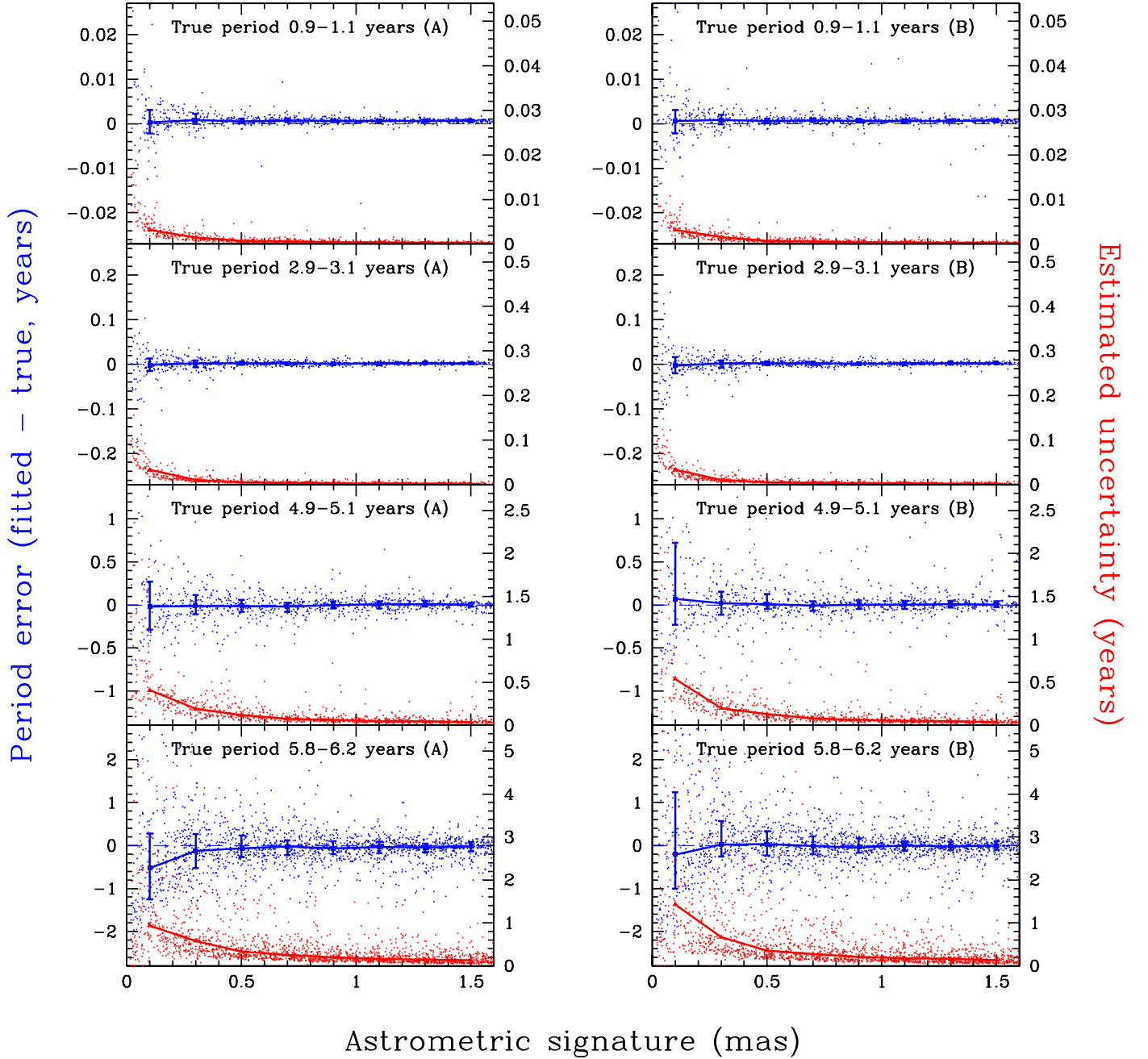


Fig. 7. Error in period as a function of astrometric signature for different period ranges and for both solvers. The dots show the difference between fitted and true period (blue, left axis) and the estimated uncertainty from the solution (red, right axis). Shown on the left panels are the solutions by Solver A, and on the right those by Solver B. Heavy dots represent the median values, binned in astrometric signature; error bars represent the interquartile range.

ity and robustness of the fits. Such a study lies beyond the scope of this work, and we leave it for future investigations.

3.2.2. Estimated and actual errors

A more quantitative analysis of the fitted parameters can be carried out by comparing the distribution of differences between true and fitted parameters with the errors estimated as part of the solution process. The distribution of differences can be used to determine the actual uncertainties in the fit, which in the ideal case would match the uncertainties estimated by the fit. In reality, this is not a perfect process; the estimated uncertainties

are based on noisy data, and therefore tend to be biased towards smaller values when the noise produces an apparently larger signal. Nonetheless, a general agreement between estimated and actual errors is to be expected for a good fitting process.

The results presented in this Section demonstrate that both Solvers are not only capable of recovering the expected signal for the overwhelming majority of the simulated orbits under the conditions of the T2 test (as shown in the previous Section), but also that error estimates are generally accurate, with the overall distribution of the difference between fitted and true parameters very close to the solution results. Some discrepancies—a bias of up to 2 sigma in estimated period and a mismatch of up to a fac-

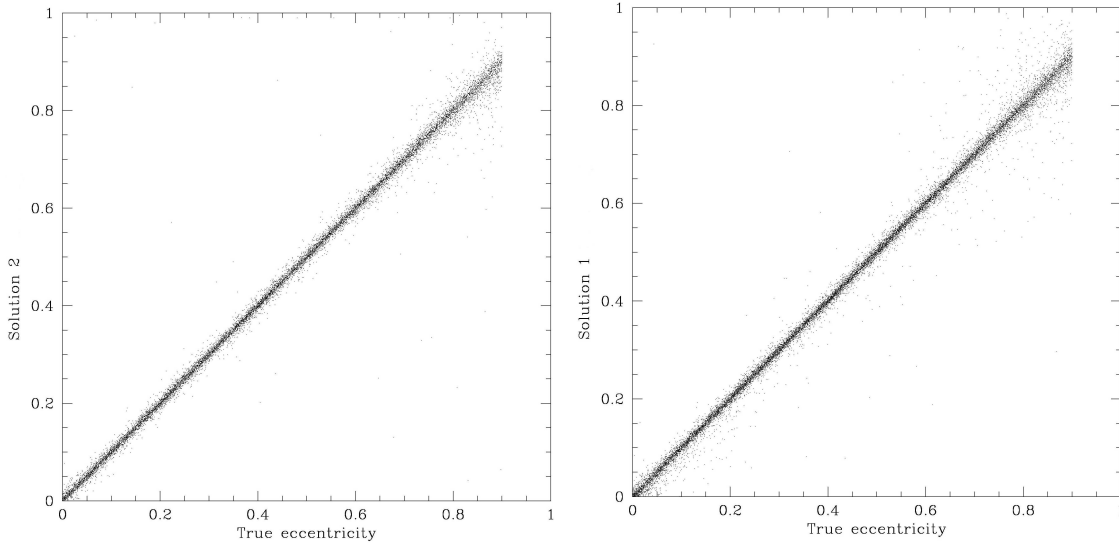


Fig. 8. Fitted vs. true orbital eccentricity for Solver A (left) and Solver B (right). Included are the orbits with signature larger than 0.4 mas—approximately 75% of the cases studied—and period shorter than 5 years.

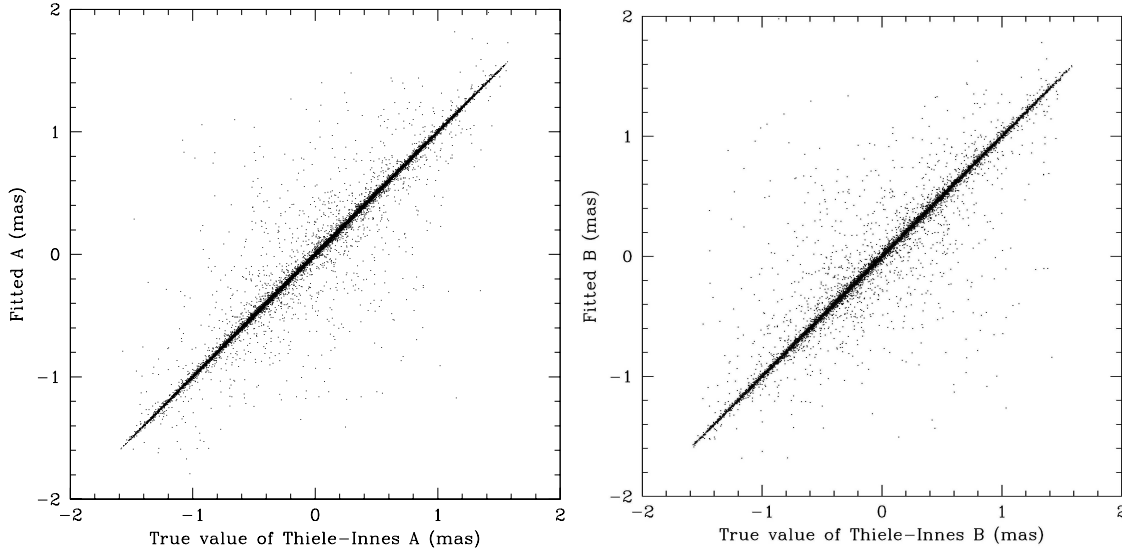


Fig. 9. Fitted vs. true values of the Thiele-Innes parameters A and B, according to the solution by Solver B. As in Figure 8, included are orbits with $\alpha > 0.4$ mas and $P > 5$ yr.

tor 2 in estimated errors—do occur under special circumstances, such as very short and very long periods. These discrepancies, small in the economy of this test, can be evaluated and corrected for by a more thorough understanding of the estimation process and its error estimates. An incorrect solution is returned for about 2% of the planets. Such cases are not identified from their formal error estimates, and will need to be addressed by a more aggressive understanding of possible aliasing in orbital parameter space. Simulations and solutions show conclusively that correct solutions with accurate error estimates can be obtained for about 98% of the simulated planets.

Indeed, the estimated and actual errors do match with good accuracy under most conditions. An indication can be seen in Figure 6, where we show that the typical difference between true and fitted period, as estimated from the interquartile range, is very close to the median estimated uncertainty for diverse values of orbital period and amplitude.

A more quantitative—and challenging—test can be carried out by studying the distribution of differences in the parameters compared with their predicted errors. Since predicted errors can in principle depend on the amplitude of the signature, period, times of observation, and other orbit details, we define the *scaled difference* as the difference between the fitted and the true value of an orbital parameter, divided by its estimated uncertainty for that same case. If the errors are predicted correctly and follow a Gaussian distribution, this quantity will also be distributed normally with zero mean and unit dispersion. Discrepancies between predicted and actual errors will show up as distortions in this distribution.

The expectation of a good error distribution should hold primarily for the cases with good signal and solid orbit reconstruction, for which the true and the reconstructed orbits are close. We therefore focus on planets with $P < 5$ years and $\alpha > 0.4$ mas, about 20,000 cases.

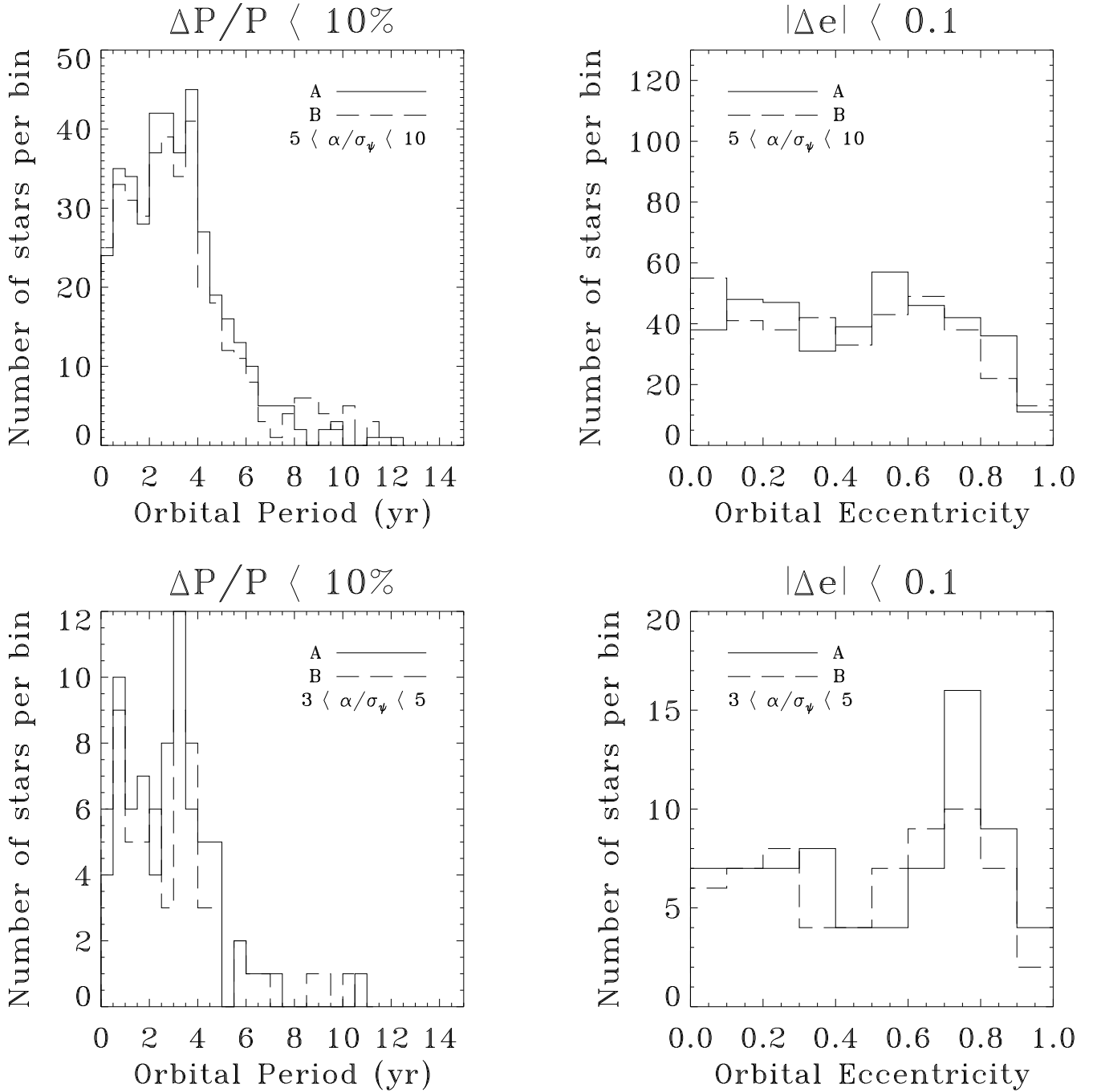


Fig. 10. Top left and right: distributions of well-measured values of P and e for the two Solvers in the case of $5 < \alpha/\sigma_\psi < 10$. Bottom left and right: the same, but for the case of $3 < \alpha/\sigma_\psi < 5$.

Figure 11 shows a definite distortion of the overall scaled difference in period for both Solver B (blue) and Solver A (red); the width of the distribution is similar to the predicted value (dashed), but the peak is shifted towards positive values (i.e., the fitted value of the period is statistically biased towards positive errors, or longer periods). The difference is small, about 0.5-sigma, but it is nonetheless statistically significant because of the large number of simulations used.

The difference in period appears to be a function of the period itself. When considering planets with different periods, it appears that the period difference decreases for longer periods, and vanishes at ~ 5 years. This appears clearly in Figure 12, where the median and interquartile scaled period difference is

binned as a function of period for both solutions. Periods shorter than 5 years are overestimated, while longer periods are underestimated. The difference remains comparable to the estimated error (one sigma), except for periods around 1 year and shorter which are overestimated by up to 2 sigma. We remind the reader that this is in part a result of the errors being very small; the typical period error at 1 year is 0.005 years (see Figure 7), so as a fraction of the period itself, this bias is typically less than a percent. Nonetheless, the fact that the difference is systematic and present in both solutions suggests that there is a conceptual issue worth of further analysis.

We next consider the distribution of linear parameters, using the Thiele-Innes B parameter in the Solver B solution as an

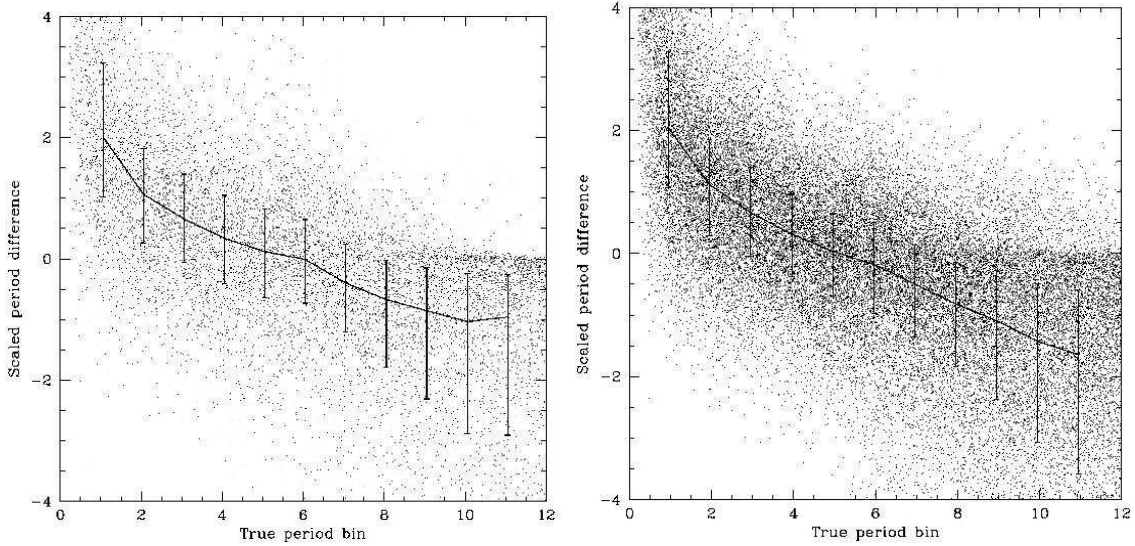


Fig. 12. Scaled period differences for Solver A (left) and Solver B (right), for all orbits with signature larger than 0.4 mas. The curve and error bar represent the median and quartiles in 1-year bins in true period.

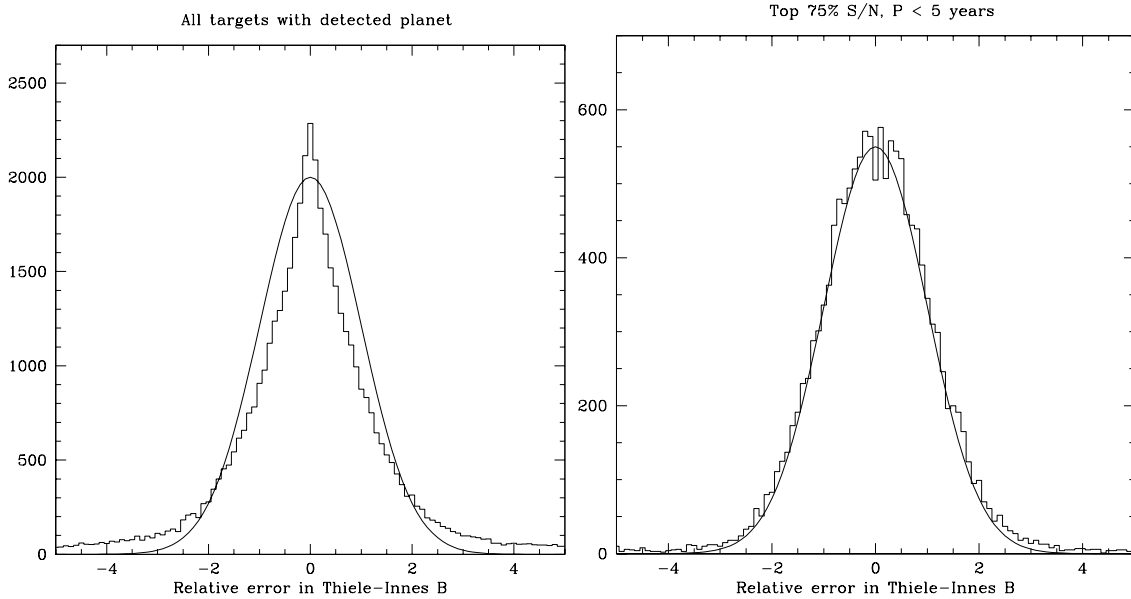


Fig. 13. Distribution of scaled difference in the Thiele-Innes parameter B for the Solver B solution. The left panel shows all data points; the right panel only the planets with signature larger than 0.4 mas and period shorter than 5 years. The dashed curve in each plot is a reference Gaussian with zero mean and unit dispersion.

example. The overall distribution of scaled errors is, not surprisingly, unbiased in the mean, and is comparable in width to the expected distribution (Figure 13, left panel). However, the observed distribution does differ from the nominal Gaussian, both for small and for large errors. The core of the distribution appears narrower than the Gaussian, indicating that errors may be overestimated for part of the distribution; on the other hand, the elevated tails—and the 2% of solutions that fall outside the 5-sigma range of the histogram—indicate that errors are underestimated for some objects.

A closer analysis shows that the narrow peak is due primarily to planets with small signatures (< 0.4 mas) and periods shorter than 5 years, while the tails are largely due to long-period planets. Figure 13, right panel, shows that the distribution of scaled differences for B for all planets with signature larger than 0.4

mas and period shorter than 5 years is very close to Gaussian, although about 2% of outliers remain.

3.3. Test T3: Multiple-planet solutions and coplanarity

The T3 experiment is designed primarily to determine how well multiple-planet systems can be identified and solved for, as well as how well the mutual inclination angle of pairs of planetary orbits can be measured. In addition, the accuracy of multiple-planet solutions will be compared with that of single-planet solutions for systems with similar properties. The noise characteristics of the data are assumed to be fully understood.

Each solver was asked to carry out a full orbital reconstruction analysis for each star, beginning from the period search and including error estimates for each of the orbital parameters. As

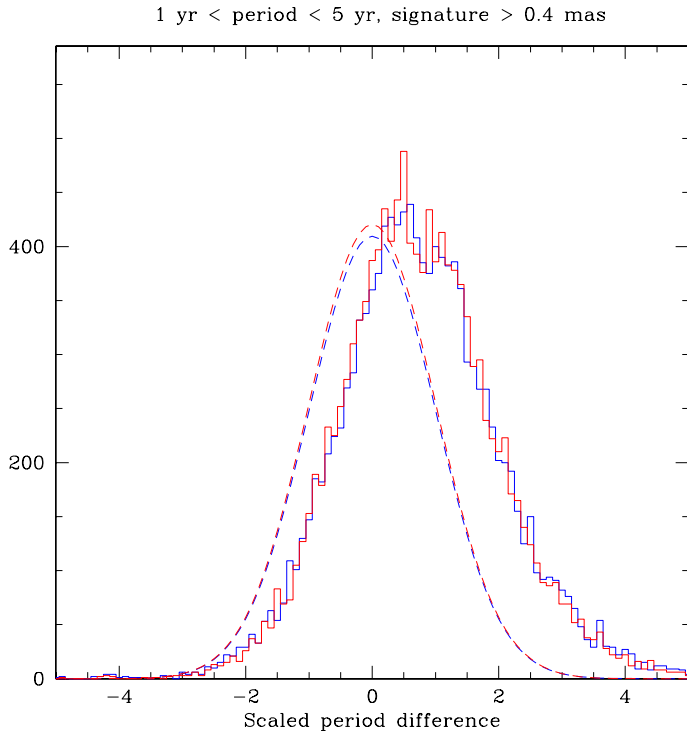


Fig. 11. Histogram of scaled period differences for planets with period between 1 and 5 years and signature larger than 0.4 mas. The red histogram is for Solver A, blue for Solver B. The dashed lines represent a Gaussian distribution with zero mean and unit dispersion.

for the T1 and T2 tests, two solvers, Solver A and Solver B, participated in this test, each with their independently developed numerical code.

Simulated data were prepared for 3,000 stars, in two separate experiments (T3a and T3b). In the two cases, respectively 310 and 307 objects had one planet, while the remaining 2690 and 2693 had two planets. In both experiments, astrometric signatures ranged between $\alpha = 16 \mu\text{as}$ (astrometric signal-to-noise $\alpha/\sigma_\psi \approx 2$) and $\alpha = 400 \mu\text{as}$ ($\alpha/\sigma_\psi \approx 50$). The first planet was always generated with a mass $M_p = 1 M_J$, and with P uniformly, randomly distributed between 0.2 and 9 years. The second planet was constrained to have P at least a factor 2 shorter or longer than the first planet, and its corresponding mass was assigned as to produce an astrometric signal falling in the above mentioned range. The orbital eccentricity was randomly distributed, but limited to the ranges $0.1 \leq e \leq 0.6$ and $0.0 \leq e \leq 0.6$ in the T3a and T3b experiments, respectively. In the first experiment, no constraints were placed on the value of the mutual inclination angle i_{rel} between pairs of planetary orbits. In the second experiment, it was constrained to be $i_{\text{rel}} \leq 10^\circ$.

Both Solvers run their respective pipelines, consisting of detection, initial parameter determination, and orbital reconstruction, on each of the 3,000 simulated time series provided by the Simulators. They have no a priori knowledge of the orbital properties of each planet, nor they know whether a star has none, one, or more planets.

In both cases, solvers use the equivalent of a least-squares algorithm to fit the astrometric data for each planet; they need to solve for the star's basic astrometric information (position, parallax, proper motion), for which only low-accuracy catalog parameters are provided, as well as for the parameters of the re-

flex motion, for each detected companion. For all planets fitted for, Solver B provides the results in the form of period P , eccentricity e , epoch of pericenter passage T , and the Thiele-Innes parameters A, B, F, G . He provides also estimated uncertainties for each parameter. Solver A also provides period, eccentricity, and pericenter passage, but instead of the Thiele-Innes parameters, he returns semi-major axis a , inclination i , position angle of the ascending node Ω , and longitude of pericenter ω . Like Solver B, he computes formal errors for each parameter.

In summary, the results presented in Sec. 3.3 demonstrate that the expected signal can be recovered for over 70% of the simulated orbits under the conditions of the T3 test (for every two-planet system, periods shorter than 9 years and differing by at least a factor of two, $2 \leq \alpha/\sigma_\psi \leq 50$, moderate eccentricities). Favorable orbital configurations (both planets with periods ≤ 4 years, both astrometric signals at least ten times larger than the nominal single-measurement error, and redundancy of over a factor two in the number of data points with respect to the number of fitted parameters) have periods measured to better than 10% accuracy > 90% of the time, and comparable results hold for other orbital elements. A modest degradation of up to 10% (slightly different for different parameters) is observed in the fraction of correct solutions with respect to the single-planet solutions of the T2 test. The useful range of periods for accurate orbit reconstruction is reduced by about 30% with respect to the single-planet case. The overall results are mostly insensitive to the mutual inclination of pairs of planetary orbits. Over 80% of favorable configurations have i_{rel} measured to better than 10° , with only mild dependencies on its actual value, or on the inclination angle with respect to the line of sight of the planets. Error estimates are generally accurate, particularly for fitted parameters such as the orbital period, while (propagated) formal uncertainties on the mutual inclination angle seem to often underestimate the true errors. Finally, it is worth mentioning how, as already shown by radial-velocity surveys, long-term astrometric monitoring, even with lower per-measurement precision, would be very beneficial for improving on the determination of multiple-planet system orbits and mutual alignment, thanks to the increasingly higher redundancy in the number of observations with respect to the number of estimated model parameters in the solutions.

3.3.1. Overall quality of the solutions

For both experiments, Solver A reports solutions for all stars. Solver A initially carries out an orbital solution for a single planet orbiting each star. He then performs a χ^2 -test on the post-fit observation residuals, at the 99.73% confidence level. This allows one to provide an initial assessment of the detectability of the signal of a second planet in the system, as a function of its properties.

For the first experiment, a total of 509 objects have $P(\chi^2) \geq 0.0027$, thus are classified as systems with only one planet. Of these, 289 out of 310 simulated ones are truly star+planet systems. Of the remaining 220 objects orbited by 2 planets but for which a single planet solution appears satisfactory, the overwhelming majority of the cases (93%) are constituted by systems in which at least one planet has P exceeding the time-span of the observations ($T = 5$ yr), and often times the inner planet has $P \approx T$. In virtually all cases, the fitted value of the period is close to that of the inner planet, or it's intermediate between that of the inner and that of the outer planet. In the 7% of cases in which both planets have $P \leq 5$ yr, one of the astrometric signatures is

always close to the detection limit ($\alpha/\sigma_\psi \leq 3$). Essentially identical results hold for the second experiment. A more thorough investigation of the behavior of false detections and of the realm of degradation of detection efficiency in presence of a second planet is beyond the scope of this report, and it will require much larger sample sizes. Finally, Solver A performs a two-planet solution on all stars. In both experiments, essentially the same fraction of systems with two planets ($\approx 73\%$) passes the χ^2 -test on the post-fit residuals, at the 99.73% level. For the remaining 27% of cases in which a two-planet solution is not satisfactory within the predefined statistical tolerances, Solver A does not attempt to fit for a three-planet configuration.

From the results reported by Solver B for the T3b experiment, 24 stars have no solution (in 85% of the cases objects with less than 25 observations). For the remaining 2976 objects, Solver B fits at least two planets, and a 3-planet orbital solution is reported for 43% of the sample. Overall, $\sim 56\%$ of the systems are correctly identified by Solver B as having only two planets, with post-fit $P(\chi^2) \geq 0.05$. The T3a experiment yielded very similar results.

Overall, only $\sim 40\%$ of the two-planet systems simulated have a good solution according to both Solvers. Simply based on the post-fit χ^2 test, the two fitting algorithms thus perform differently in a measurable fashion, unlike the T2 test case, in which the performance of the two codes for single-planet orbital fits was essentially identical.

The next steps are to focus on good ($P(\chi^2) \geq 0.0027$ for Solver A, $P(\chi^2) \geq 0.05$ for Solver B) two-planet solutions reported by the Solvers when the simulated systems are truly composed of two planets, and investigate a) how well solvers actually recover the orbital parameters of the planets, b) how the quality of multiple-planet solutions compares with that of single-planet fits for planets with comparable properties, and c) how accurately the actual value of the mutual inclination angle i_{rel} is recovered in the case of quasi-coplanar and randomly oriented pairs of planetary orbits.

3.3.2. Multiple-Keplerian orbit reconstruction

The relative performances of Solver A's and B's algorithms in accurately recovering the orbital parameters in the case of two-planet systems are quantified using the results for the orbital period of the two planets. This is the most important of the orbital parameters, and the most critical in terms of obtaining an orbital solution that is close to the truth. As already noted above, we find that the overall performance in multiple-planet orbit reconstruction does not depend significantly on the relative alignment of the orbits, so that we present here results from the T3b experiment, i.e. the quasi-coplanar orbits case.

The first noticeable result are the large differences in the distributions of orbital parameters for the two Solvers. Figure 14 shows, compared to the true simulated ones (solid histograms), the recovered distributions of orbital periods of the first and second planet. In the upper four panels, the results for all stars (excluding objects with only one planet, but for Solver B including those for which three planets are fitted) are presented for both Solvers. In panels five and six, Solver B's results are shown only for stars with good two-planet solutions, while in the last two panels Solver B's distributions of periods of the second and third planet are presented, for the sample of stars with three-planet orbital solutions.

On the one hand, for Solver A's solutions (panels 1 and 2) the most obvious feature observed is the fact that in a significant number of orbital solutions the periods are swapped (roughly

30% of the cases, averaging over all periods), i.e. the first planet identified in the data is the second generated in the simulations, and vice-versa. This result is easily understood, as, given the simulation setup, the dominant signal (identified by, for example, a better sampled period, or a larger astrometric signature) is not necessarily the one of the first planet generated. Otherwise, Solver A's solutions appear to recover reasonably well the true underlying distributions.

On the other hand, for Solver B's solutions no obvious pattern of this kind can be found. Instead, over 1/3 of the periods identified as dominant is within 0.5 years, and no periods greater than 5 years are identified (panel 3). The former feature is in common to the solutions for the second planet (panel 4). When only two-planet solutions (with good post-fit $P(\chi^2)$) are considered (panels 5 and 6), the recovered distributions still look largely different from those obtained by Solver A and from the true ones. Finally, as it appears clear by comparing panels 7 and 8, and 5 and 6, the vast majority of short-period period orbits fitted for the second planet ($\sim 90\%$), and $\sim 50\%$ of those for the first planet, seems to be the undesired consequence of three-planet fits, with a correspondingly very large number of long periods found for the third planet.

Such differences translate in a lower percentage of correctly identified two-planet systems by Solver B (even when the post-fit χ^2 -test is satisfactory). In fact, in Figure 15 we show the distributions of true periods for the first and second planet compared to the fitted distributions when the value of the period falls within 10% of the simulated one. In order to compare results between the two Solvers in almost identical conditions, for Solver A only stars with post-fit $P(\chi^2) \geq 0.05$ are included, while for Solver B only two-planet solutions are considered (all having $P(\chi^2) \geq 0.05$). Overall, Solver B's algorithm performs about 40% worse than Solver A's (for the first and second planet respectively, 554 and 807 stars satisfy the above constraints for Solver B, while for Solver A the equivalent numbers are 993 and 1223). This difference increases to over a factor of two if Solver A's $P(\chi^2) \geq 0.0027$ criterion is adopted. The number of stars with both periods simultaneously satisfying the above conditions is also lower for Solver B, by some 15%. It is true that about 10% of the stars for which Solver B performs three-planet fits actually have the orbital period of the first and second planet fitted falling within the above-mentioned criteria, thus helping to somewhat reduce the observed discrepancy in performance. However, we will only focus on Solver A's $\sim 70\%$ of good two-planet orbital solutions (at the 99.73% confidence level), a total of 1912 and 1900 stars for the T3a and T3b tests, respectively. Focusing on Solver A's cleaner, and larger, sample of good orbital solutions allows one to effectively undertake the comparison between the T2 and T3 tests, by using stellar samples for which orbital solutions have comparable quality.

3.3.3. Comparison with test T2

We use orbital period and eccentricity as proxies to understand the behavior of the two-planet orbital solutions, and compare them with analogous results obtained in the T2 experiment. The properties of good two-planet solutions should thus be easier to understand.

For the T3b case (quasi-coplanar orbits), the four panels of Figure 16 show, as a function of the value of the true orbital period, the fraction of stars with good orbital solutions for which the periods of both planets are recovered by Solver A with a fractional uncertainty $\Delta P/P \leq 10\%$ (where ΔP is the difference between fitted and true period value). For comparison, analogous

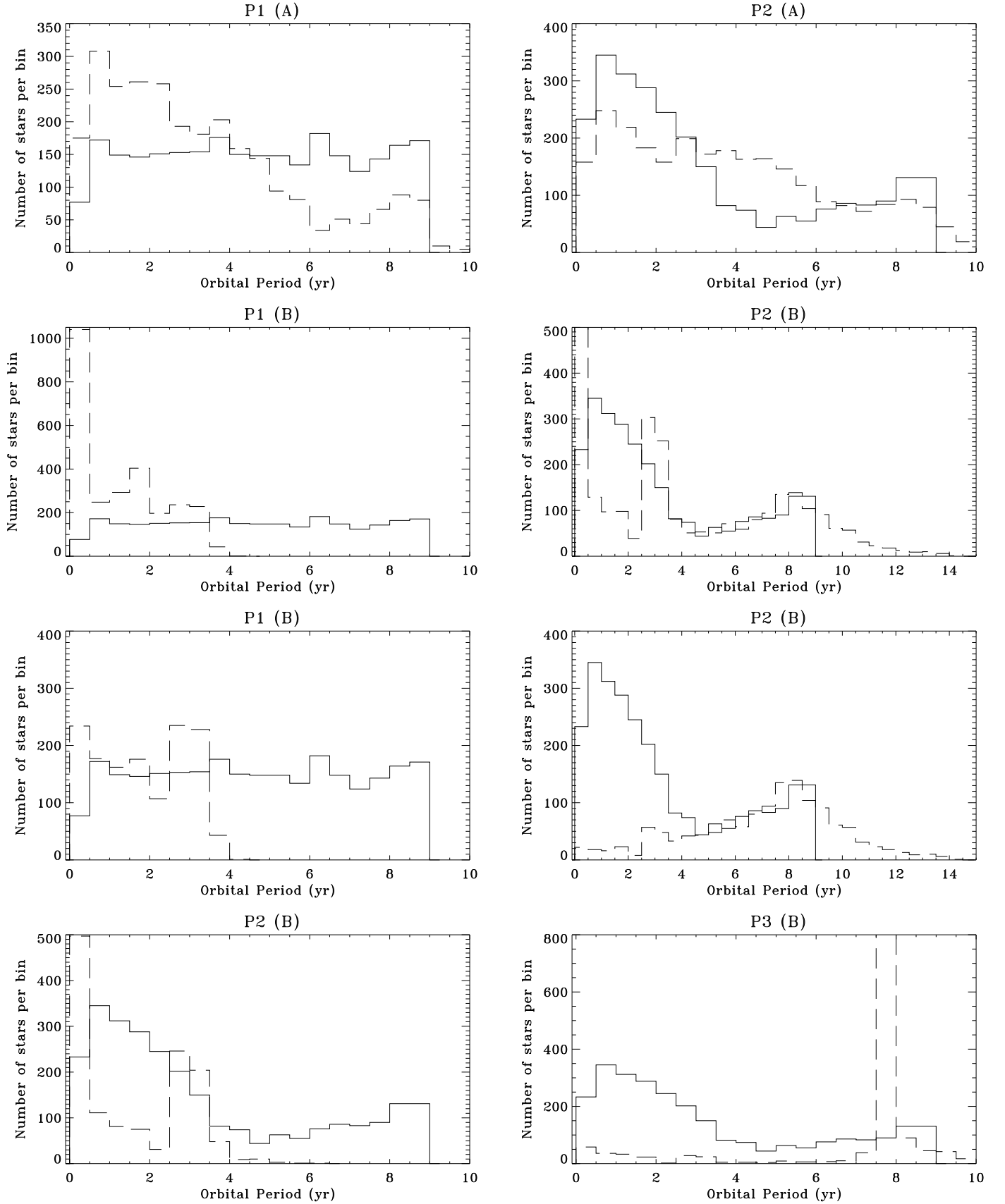


Fig. 14. Distribution of orbital periods in the multiple-planet solutions (dashed and dashed-dotted lines), compared with the true underlying distributions (solid lines). Top two panels: results for planet 1 and 2 obtained by Solver A (all stars). Panels 3 and 4: the same for Solver B, including stars with both two and three planets found. Panels 5 and 6: the same for Solver B, but excluding stars with three planets fitted. Bottom two panels: the true distribution of the second planet compared with the same distributions for planet two and three obtained by Solver B in the sample of three-planet orbital fits.

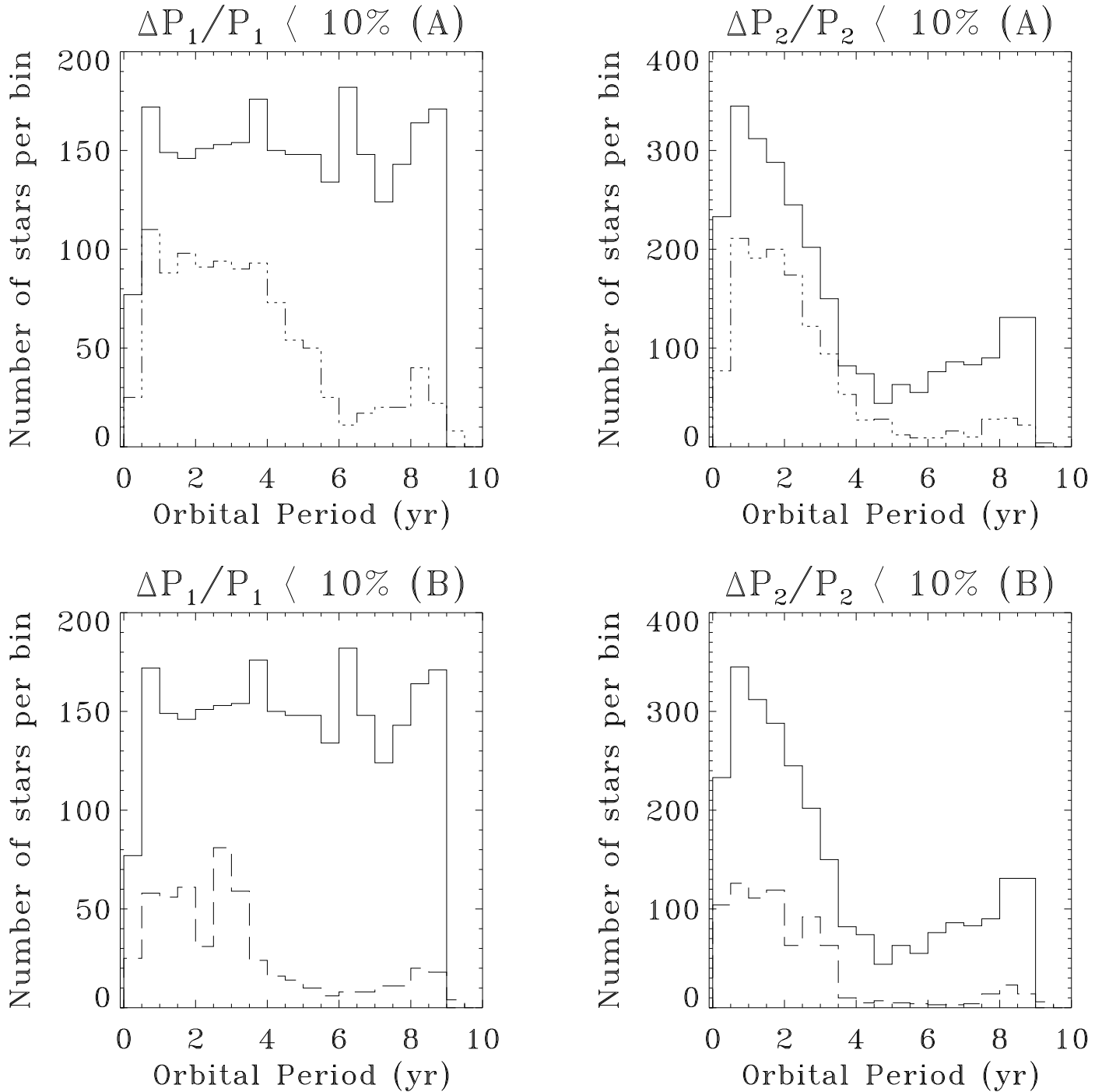


Fig. 15. True distributions for planet 1 and 2 (solid histogram) compared with the same distributions derived by Solver A (top two panels) and Solver B (bottom two panels) when the fitted values of the periods lie within 10% of the simulated values.

results from the T2 experiment are over-plotted, after constraining orbital periods, eccentricities, and astrometric signals to lie in the same ranges of the T3b experiment ($P \leq 9$ yr, $e \leq 0.6$, and $\alpha \leq 400 \mu\text{as}$).

Overall, the quality of the solutions degrades quickly already for periods ≥ 2 years, and the fraction of systems with both orbital periods recovered to within 10% of the true value is at least 5%-10% lower than the single-planet case. For configurations in which both planets have $P \leq 5$ yr, $\alpha/\sigma_\psi \geq 10$, and for which a number $N_{\text{oss}} \geq 45$ of observations are carried out over the 5-yr simulated mission lifetime (bottom right panel), the situation

improves significantly. Over 90% of all orbital configurations have both periods measured to better than 10%, and the 5%-10% deficit with respect to the T2 experiment applies for periods in the range $0.2 \leq P \leq 4$ yr, for both planets in the systems. A very similar behavior is observed (but not shown) in the T3a experiment, in which no constraints are put on the mutual inclination angles.

Formal errors from the fitting procedure appear to match the actual errors reasonably well. To determine more quantitatively how good an approximation the estimated errors are for the true ones, we utilize the same metric adopted in the T2 experiment,

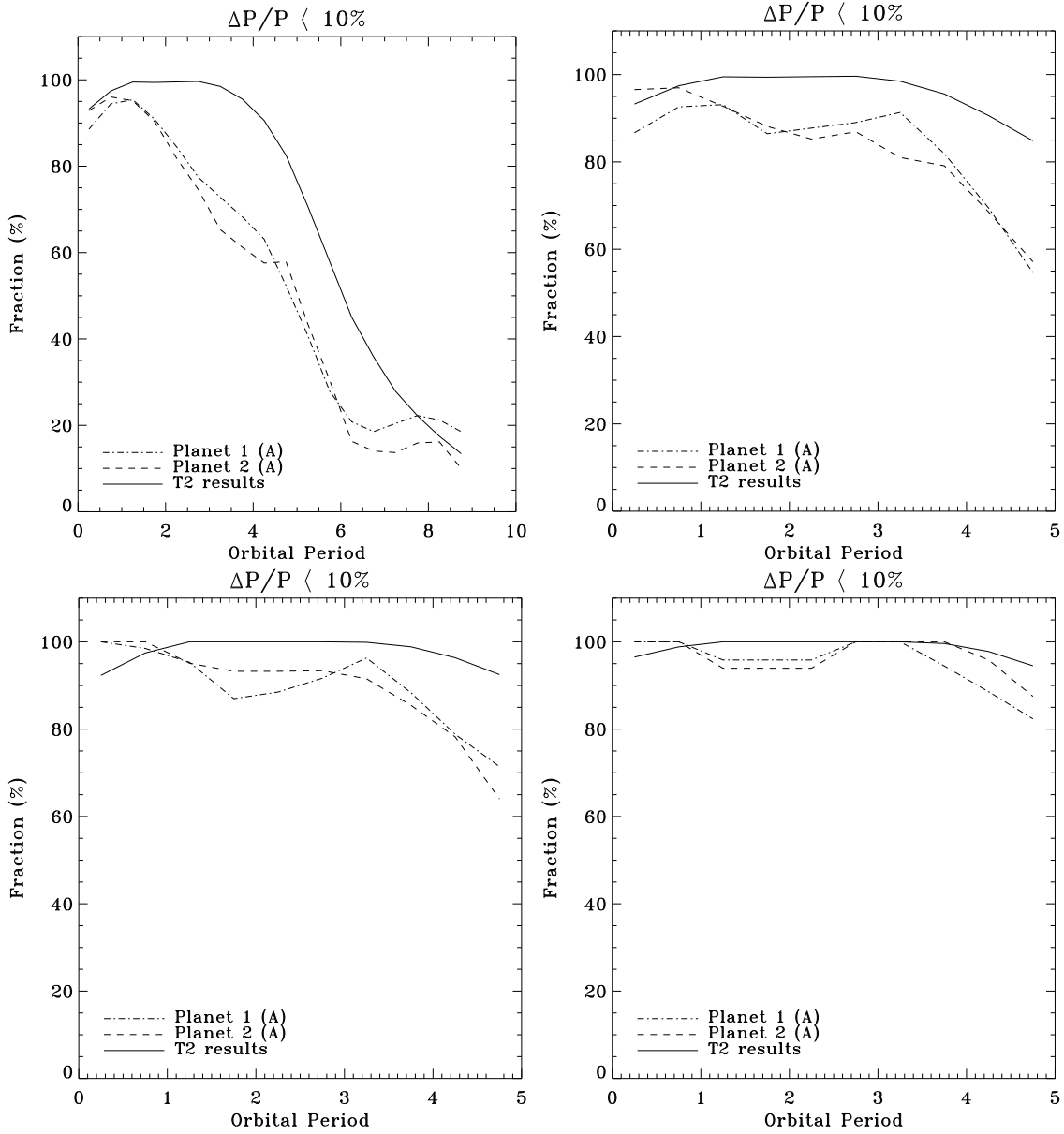


Fig. 16. Fraction of systems with good orbital solutions ($P(\chi^2) \geq 0.0027$) in the T3b experiment for which both orbital periods are recovered by Solver A with a fractional uncertainty $\leq 10\%$, as a function of period (0.5-yr bins). For comparison, the same results are displayed for the T2 test. Top left: all stars. Top right: systems with both periods ≤ 5 yr. Bottom left: systems with both periods ≤ 5 yr, and with $\alpha/\sigma_\psi \geq 10$. Bottom right: systems with both periods ≤ 5 yr, $\alpha/\sigma_\psi \geq 10$, and with $N_{\text{oss}} \geq 45$.

i.e. the scaled difference $\Delta P_j/\sigma_{P_j}$ ($j = 1, 2$) defined as the ratio between the fitted and the true value of the orbital period of the j -th planet and its corresponding formal uncertainty. We limit ourselves to the sample of stars for which Solver A obtains good solutions (99.73% confidence level), and for which orbital periods are recovered to within 10% accuracy. Figure 17 shows that, for both planets, and in both the T3a and T3b experiment, the distributions of scaled period differences are quite close to the predicted value (a Gaussian with zero mean and unit dispersion). A small shift in the peak of the $\Delta P/\sigma_P$ distribution for the second planet in the T3b test might be present, but its statistical significance is low. Elevated tails, however, indicate that a non-negligible fraction of objects have underestimated periods (7% of the objects lie above the $3\text{-}\sigma$, and 2% above the $5\text{-}\sigma$ threshold out of the scale of the plot in Figure 17).

Finally, the two panels of Figure 18 show results for the eccentricities of both planets in the systems. Displayed are the fractions of systems with good orbital solutions for which the fitted values of e are within 0.05 of the true value, the left panel displaying results from the full sample with good orbital solutions, and the right after applying the above-mentioned constraints on periods, astrometric signal, and number of observations. Overall, for both planets a degradation of $\sim 20\%$ between the single-planet and the two-planet solutions is observed, independently of the actual value of e . Favorable configurations have e determined within 0.05 of the true value about 80% of the time, with a degradation of $\sim 10\%$ with respect to the single-planet solutions of the T2 test, in line with what is found for the orbital periods. The modest degradation of $\sim 5\% - 10\%$ in the fraction of well-measured periods and eccentricities with respect to the result of the T2 test is likely due to the increased number of parameters

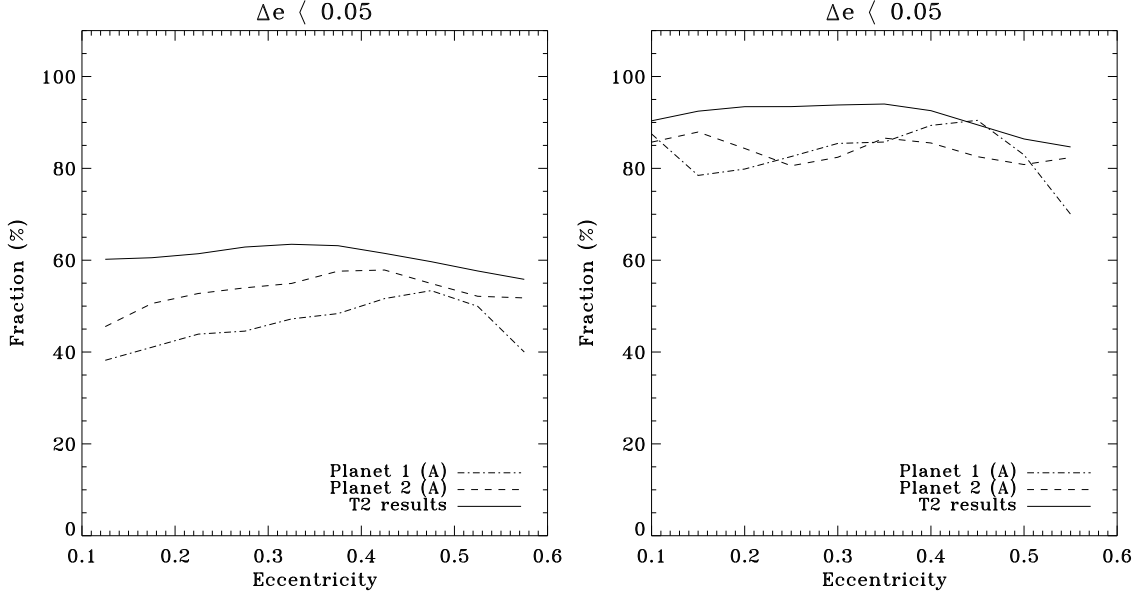


Fig. 18. Left: Fraction of systems with good orbital solutions ($P(\chi^2) \geq 0.0027$) in the T3b experiment for which both eccentricities are determined within 0.05 of the true values. For comparison, analogous results for the T2 test sample are displayed. Left: all stars. Right: systems with both periods ≤ 5 yr, with $\alpha/\sigma_\psi \geq 10$, and with $N_{\text{oss}} \geq 45$.

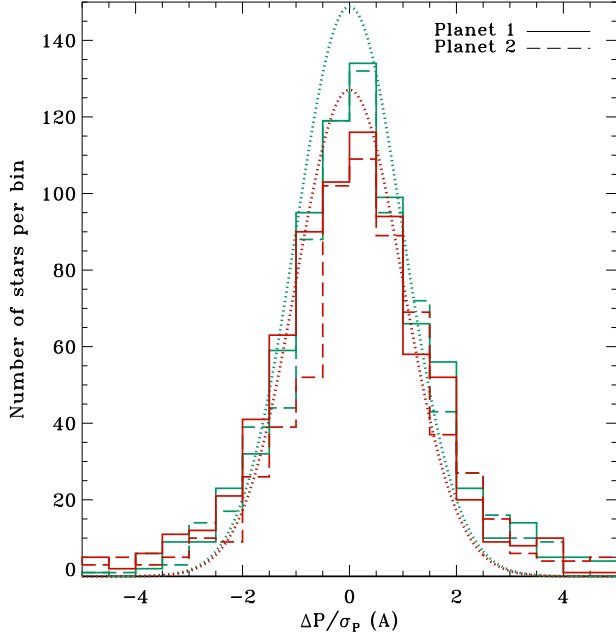


Fig. 17. Histogram of scaled period differences $\Delta P/\sigma_P$ for good two-planet fits ($P(\chi^2) \geq 0.0027$) with periods accurate to better than 10% for the T3a (green solid and dashed lines) and T3b (red solid and dashed lines) experiments. The dotted curves are reference Gaussians with zero mean and unit dispersion.

in the two-planet fits (19 vs. 12 in the single-planet solutions), given the same number of observations. Other orbital parameters follow similar patterns. And again, essentially identical results are obtained for the T3a test, demonstrating that the relative alignment between pairs of planetary orbits does not seem to play a significant role in terms of the ability of Solver A's algorithm to reconstruct with good accuracy the orbits of both planets, under favorable conditions.

3.3.4. Coplanarity measurements

The mutual inclination i_{rel} of two orbits is defined as the angle between the two orbital planes, and is given by the formula:

$$\cos i_{\text{rel}} = \cos i_{\text{in}} \cos i_{\text{out}} + \sin i_{\text{in}} \sin i_{\text{out}} \cos(\Omega_{\text{out}} - \Omega_{\text{in}}), \quad (1)$$

where i_{in} and i_{out} , Ω_{in} and Ω_{out} are the inclinations and lines of nodes of the inner and outer planet, respectively. The value of i_{rel} is thus a trigonometric function of i and Ω of both planets, and the latter two are in turn derived as non-linear combinations of the four Thiele-Innes elements, which are the actual parameters fitted for in the orbital solutions. It is thus conceivable that any uncertainties in the determination of the linear parameters in the two-planet solutions might propagate in a non-trivial manner onto the derived value of i_{rel} , and consequently a value of mutual inclination angle close to the truth might be more difficult to obtain.

In the top two panels of Figure 19 we show the fraction of stars with good orbital solutions in the T3a and T3b experiments for which the derived value of the mutual inclination angle i_{rel} is determined within 10° of the true one by Solver A. The results are expressed as a function of i_{rel} itself. Overall, for Solver A both experiments give similar results, showing that his fitting algorithm is only mildly sensitive to the mutual inclination of pairs of planetary orbits.

In both cases, Solver A globally recovers $\sim 40\%$ of the i_{rel} values to within 10° uncertainty, independently of the value of mutual inclination. The fraction of systems for which the actual value of i_{rel} is determined within the above tolerance increases when the constraints on well-sampled, high signal-to-noise orbits, with a sufficient number of observations, are set, up to 90% . In the top left panel of Figure 19, both ends of the upper three curves are not significant, due to very low number statistics considerations. Actually, the results shown in the top right panel can be mapped in the top left panel (at least for $2^\circ \leq i_{\text{rel}} \leq 10^\circ$), thus highlighting that the apparent quick degradation in the fraction of systems with i_{rel} accurately determined is not real. It does nevertheless appear that, for random mutual orientation of the orbits,

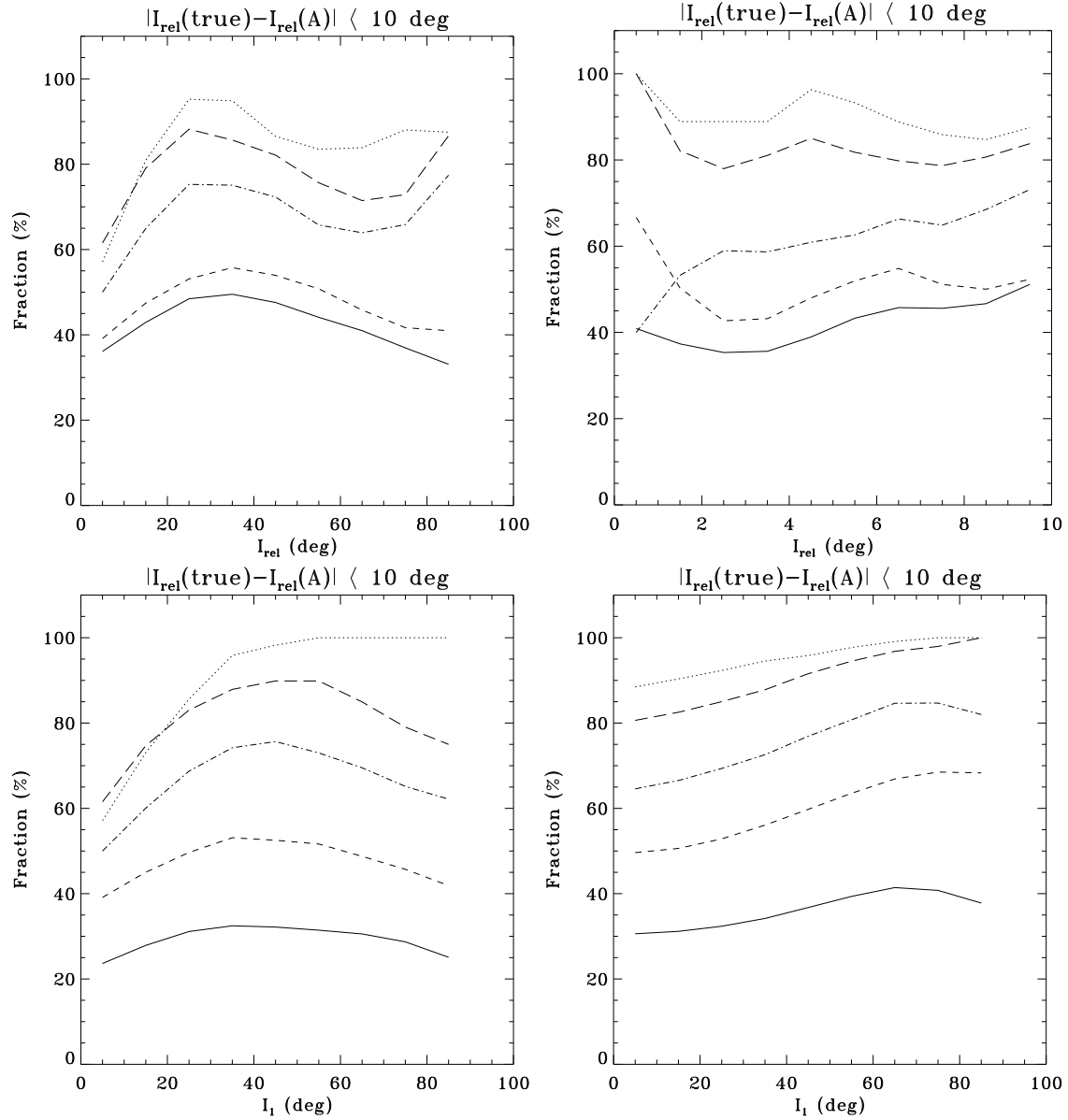


Fig. 19. Top left: Fraction of systems in the T3a experiment with satisfactory goodness-of-fit ($P(\chi^2) \geq 0.0027$) for which i_{rel} is determined to within 10° of the true value, as a function of i_{rel} itself (10 deg bins). Top right: the same for the T3b test (1 deg bins in i_{rel}). Solid lines: all stars; dashed line: both orbital periods ≤ 5 years; dashed-dotted line: $\alpha/\sigma_\psi \geq 10$; long-dashed line: both orbital periods ≤ 5 years and $\alpha/\sigma_\psi \geq 10$; dotted line: both orbital periods ≤ 5 years, $\alpha/\sigma_\psi \geq 10$, and $N_{\text{oss}} \geq 45$. Bottom left and right: Same as the top two panels, this time as a function of the inclination angle of one of the two planets.

values of i_{rel} between 30° and 40° are slightly more likely to be identified correctly (by some 20%) than quasi-coplanar cases or cases with i_{rel} close to 90° . For the quasi-coplanar case, perfectly coplanar orbits are slightly less likely to be correctly identified.

The two lower panels of Figure 19 show similar results, but this time expressed as a function of the inclination angle of one of the two planets. Again, Solver A's results for the T3a and T3b sample are similar in terms of fractions of systems with i_{rel} correctly identified within 10° of the true value, when the various constraints are applied. However, the fraction of quasi-coplanar orbits correctly identified seems to be systematically higher, by up to 10%, than those with random values of i_{rel} , except for the region with inclination angles in the intermediate range 30° – 50° , in which random values of i_{rel} , away from face-on or edge-on

configurations, appear to be somewhat favored (by up to 20% more). Configurations in the T3a experiment in which one of the two planets is seen almost face-on appear unfavorable particularly when high signal-to-noise, well-sampled orbits are considered. A similar, but less significant (differences up to 10%), trend is seen for the case of the T3b experiment (orbits viewed close to face-on are less likely to have i_{rel} measured accurately than quasi edge-on configurations). The responsible for such an effect is not, however, small-number statistics. That determining precisely the value of i_{rel} for almost face-on orbits is somewhat more difficult should not in fact come as a surprise, as this result had already been discussed in our previous papers on Gaia and SIM multiple-planet detection and orbit determination (Sozzetti et al. 2001, 2003b). When $i \rightarrow 0^\circ$, the uncertainty on the position angle of the line of nodes grows, as eventually Ω becomes

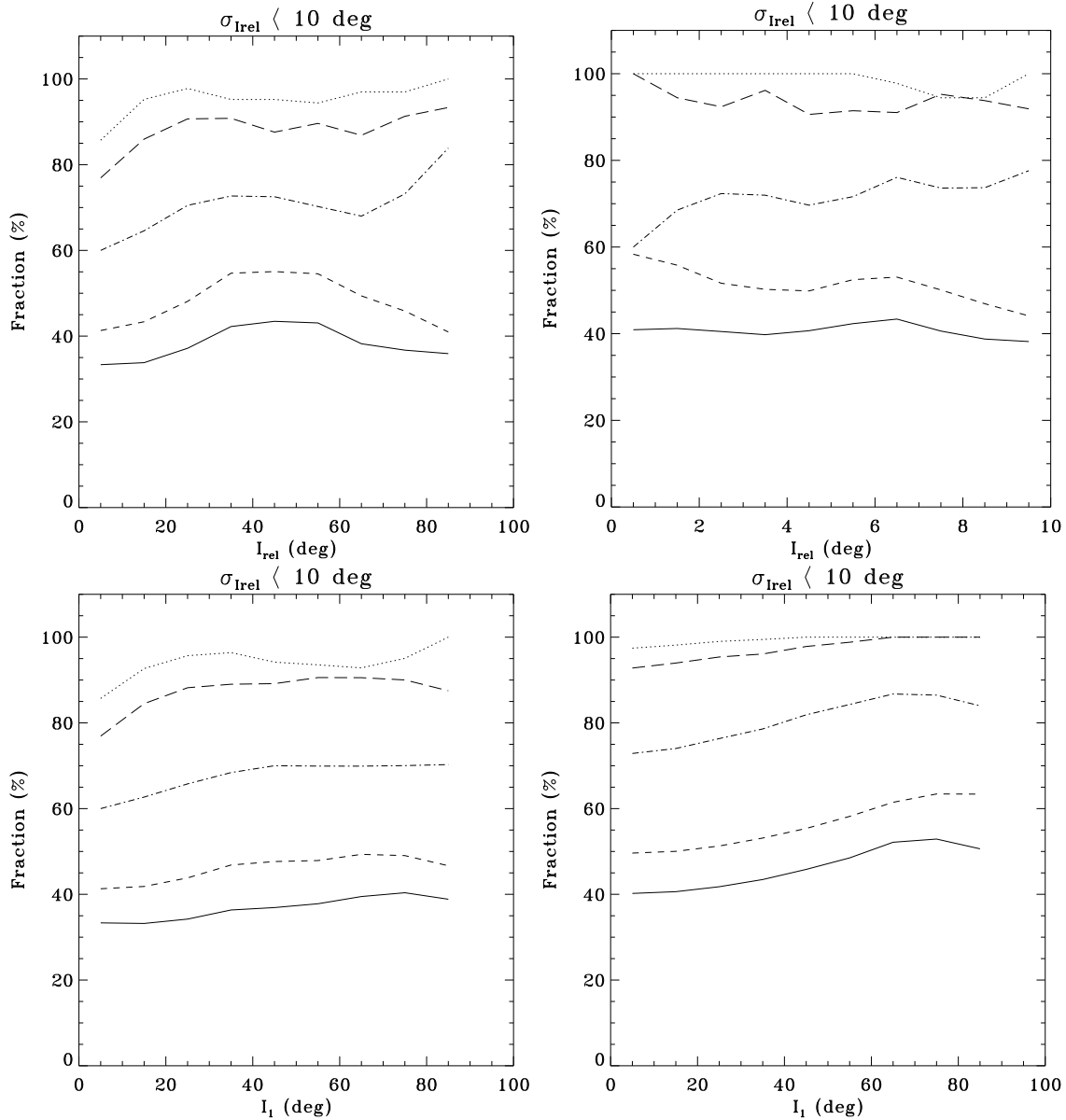


Fig. 20. Top left and right: Same as the two upper panels of Figure 19, but for the formal uncertainties on i_{rel} as calculated by propagating the formal errors on the Thiele-Innes elements from the covariance matrix of the solutions. Bottom left and right: Same as the two lower panels of Figure 19, but for the formal uncertainties on i_{rel} calculated as for the top two panels.

undefined for $i = 0^\circ$. If one of the two planetary orbits is close to face-on, but i_{rel} is large, then the incorrect identification of Ω is reflected in a poorer determination of i_{rel} . The effect is less severe if the two orbits are quasi-coplanar, because in this case, as $i \rightarrow 0^\circ$ for both planets, the term depending on Ω in equation 1 becomes very small, and ultimately an accurate knowledge of Ω is not required.

Finally, in Figure 20 we show the behavior of the nominal uncertainties on i_{rel} obtained by propagating the formal errors on the Thiele-Innes elements from the covariance matrix of the solutions. The results are plotted as a function of i_{rel} (upper panels) and i of one of the two planets (lower panels). The nominal uncertainties appear to follow rather closely the actual errors. We note, however, that in several cases formal errors seem to underestimate the real ones. This effect is highlighted by systematically higher fractions of objects with low values of the nominal

errors with respect to the real ones. This mild trend is observed for all values of i_{rel} and i , and in both experiments.

3.4. Directions for future work

Several complex issues have been left aside in the preliminary analyses carried out for all experiments of the double-blind tests program, such as correlations between orbital parameters and their errors, more thorough investigations of how well formal errors map the real ones, or in-depth studies of the conditions in which two-planet orbital fits are more likely to fail (e.g., due to covariance between proper motion solutions and long-period orbits). These topics will require rather sophisticated approaches and a more aggressive understanding of correlations and aliasing in orbital parameter space, and significantly larger sample sizes.

Another area of potential improvement concerns the possibility to explore alternative methods for orbit fitting to improve

on the interpretation of the observations and ultimately the inferences concerning the overall population of planets. One possible venue could be the evaluation of the applicability of Bayesian model selection, based on Markov chain Monte Carlo algorithms (e.g., Ford & Gregory 2007), to simulated Gaia data, in order to gauge their potential for accurate characterization of orbital parameters and their uncertainties.

The understanding of the technical specifications of the Gaia satellite and its astrometric instrument will develop further with time, therefore some of the simplifying assumptions in our simulations will be progressively relaxed and a more realistic error model (e.g., including zero-point uncertainties, calibrations errors, chromaticity effects, attitude error) and a realistic error distribution for ψ , including bias and magnitude terms, adopted.

Finally, there is margin for adding more realism to our reference model of planetary systems, by considering actual distributions of orbital parameters and masses, and up-to-date values of planetary frequencies. We will include some degree of mutual dynamical interactions in representative cases of planetary systems, and evaluate in detail the impact of possible sources of astrometric noise that might pollute and/or mimic planetary signatures (e.g., binarity of the parent star, stellar spots, and protoplanetary disks, whose impact can be seen in terms of additional dynamical perturbations as well as contamination by scattered light).

4. Discussion: Gaia in context

The striking properties revealed by the observational data on extrasolar planets (for a review, see e.g. Udry et al. 2007) reflect the complexities inherent in the processes of planet formation and evolution. The comparison between theory and observation has shown that several difficult problems are limiting at present our ability to elucidate in a unified manner all the various phases. Rather, one often resorts to attempt to investigate separately limited aspects of the physics of planet formation and evolution using a ‘compartmentalized’ approach.

However, improvements are being made toward the definition of more robust theories capable of simultaneously explaining a large range of the observed properties of extrasolar planets, as well as of making new, testable predictions. To this end, help from future data obtained with a variety of techniques will prove invaluable. In light of the results of the double-blind tests campaign presented in the previous sections, we focus here on the potential of high-precision global astrometry with Gaia, as compared to other planet detection methods, to help answer several outstanding questions in the science of planetary systems.

4.1. Gaia discovery space

We show in Figure 21 a summary of the results presented in the previous sections, in terms of the minimum astrometric signature required for detection and measurement of orbital parameters and masses with Gaia, as a function of the orbital period of the companion, and averaging over all other orbital parameters.

The curves in Figure 21 correspond, respectively, to iso-probability contours for 95% efficiency (virtual completeness) in detection at the 99.73% confidence level, 50% probability of measuring the companion mass to better than 15% accuracy, and for the same likelihood of measuring eccentricities with uncertainties lower than 0.1 and the inclination angle of the orbital plane to better than 10° accuracy. All curves are polynomial fits to the actual iso-probability curves, with extrapolations for val-

ues of $P < 0.2$ yr and $P > 12$ yr, i.e. out of the period range covered by our simulations. For comparison, the minimum astrometric signatures (assuming $\sin i = 1$) and orbital periods of the present-day planet sample are overplotted. The plot, which closely resembles those presented in our earlier works (Lattanzi et al. 2000a; Sozzetti et al. 2002) indicates that Gaia would detect $\sim 55\%$ of the extrasolar planets presently known (the exact fraction depending on the actual value of $\sin i$), and for $> 50\%$ of these it would be capable of accurately measuring orbital parameters and actual masses.

However, ongoing and planned surveys for planets with a variety of techniques are being designed to embrace the three-fold goal of 1) following-up and improving on the characterization of the presently known extrasolar planet sample, 2) targeting more carefully defined and selected stellar samples, and 3) covering new areas of the planet discovery space, with the ultimate expectation of eventually reaching the capability to discover Earth-sized planets in the Habitable Zone (e.g., Kasting et al. 1993) of nearby stars. Indeed, by the time Gaia flies various other observatories will be operational, gathering additional information on the already known extrasolar planets sample and producing a wealth of new discoveries. For example, both ground-based as well as space-borne instrumentation for astrometric planet searches is being developed, such as VLTI/PRIMA (Delplancke et al. 2006) and SIM PlanetQuest, with targeted single-measurement precision comparable to, if not higher than, Gaia’s. Then, the most effective way to proceed in order to gauge the relative importance of the Gaia global astrometric survey is not by looking at its discovery potential *per se*, but rather in connection with outstanding questions to be addressed and answered in the science of planetary systems, thus helping to discriminate between proposed models of planet formation and evolution.

By doing so, one immediately realizes that Gaia’s most unique contribution will likely reside in the unbiased and complete magnitude limited census of stars of all ages, spectral types, and metallicity in the solar neighborhood that could be screened for *new* planets, rather than on the additional insight its measurements might give on *already discovered* planets. In order to quantify our statement, we convert the results in Figure 21 in the equivalent range of companion masses and semi-major axes that could be detected and measured orbiting a star of given mass and at a distance from the Sun. For illustration, we show in Figure 22 Gaia’s discovery space in the $M_p - a$ plane for 3σ detection (with 95% probability) and for accurately measuring $> 50\%$ of the time orbital elements and masses of planets orbiting a $1-M_\odot$ star at 200 pc, and a $0.5-M_\odot$ M dwarf at 25 pc (objects with $V < 13$, for which Gaia’s highest astrometric precision can be achieved). From the Figure, one would then conclude that Gaia could discover and measure massive giant planets ($M_p \gtrsim 2 - 3 M_J$) with $1 < a < 4$ AU orbiting solar-type stars as far as the nearest star-forming regions, as well as explore the domain of Saturn-mass planets with similar orbital semi-major axes around late-type stars within 30-40 pc. Particularly for the latter case, the Gaia sensitivity nicely complements at wider separations the area of the discovery space covered by ground-based transit photometry and decade-long Doppler surveys (see caption for details).

4.1.1. How many planets will Gaia find?

To better gauge the Gaia potential for planet discovery, we update the early results of Lattanzi et al. (2000b), and re-compute the number of possible planetary systems within Gaia’s grasp using estimates of the stellar content in the solar neighborhood and our present-day understanding of the giant planet frequency

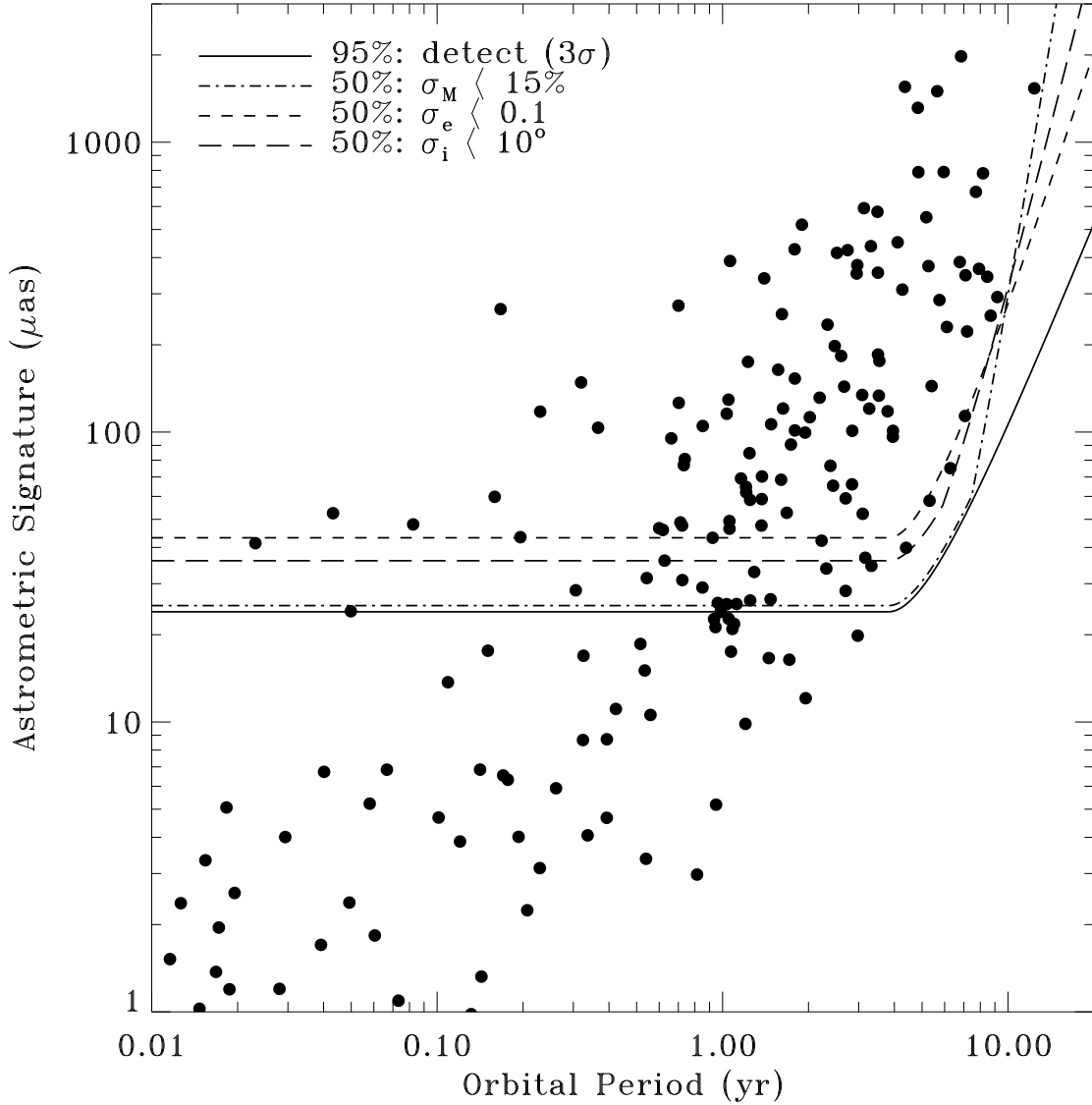


Fig. 21. Boundaries of secure ($\approx 3\sigma$, for $\sigma = 8 \mu\text{as}$) detection and accurate mass and orbital parameters determination with Gaia compared to the known extrasolar planets (data from <http://exoplanet.eu>), which are plotted for the minimum case: orbit viewed edge-on, true mass equals radial velocity minimum mass, and astrometric signature minimum. Lines of different shape represent the minimum astrometric signature for 95% probability of a 3σ detection (solid line), the minimum astrometric signature needed to determine at least 50% of the time the mass of a planet with better than 15% accuracy (dash-dotted line), the eccentricity with uncertainties < 0.1 (short-dashed line), and the inclination angle with uncertainties $< 10^\circ$ (long-dashed line), respectively. The true astrometric signature, which is proportional to the true mass, will be generally higher, much higher in some cases, with the effect that more reliable detections and orbital fits will be possible.

Table 2. Number of giant planets detected and measured by Gaia.

Δd (pc)	N_\star	Δa (AU)	ΔM_p (M_J)	N_d	N_m
0-50	$\sim 10\,000$	1.0 - 4.0	1.0 - 13.0	~ 1400	~ 700
50-100	$\sim 51\,000$	1.0 - 4.0	1.5 - 13.0	~ 2500	~ 1750
100-150	$\sim 114\,000$	1.5 - 3.8	2.0 - 13.0	~ 2600	~ 1300
150-200	$\sim 295\,000$	1.4 - 3.4	3.0 - 13.0	~ 2150	~ 1050

distribution f_p . For the former, we use the Besancon model of stellar population synthesis (Bienaymé et al. 1987; Robin & Crézé 1986), constrained to $V < 13$, and for spectral types earlier than K5. According to this Galaxy model, we should expect $N_\star \sim 15\,000$, $\sim 61\,000$, $\sim 175\,000$, and $\sim 470\,000$ stars within radii of 50 pc, 100 pc, 150 pc, and 200 pc, respectively (see Figure 23). For f_p , we take the Tabachnik & Tremaine (2002) approach, and use a power-law functional form to integrate a differential fraction within an arbitrary range of M_p and P :

$$df_p = CM_p^\beta P^\gamma dM_p dP \quad (2)$$

We find the normalization C by using the Tabachnik & Tremaine (2002) values for the exponents ($\beta = -1.1$, $\gamma = -0.73$), which still provide a good description for the observed

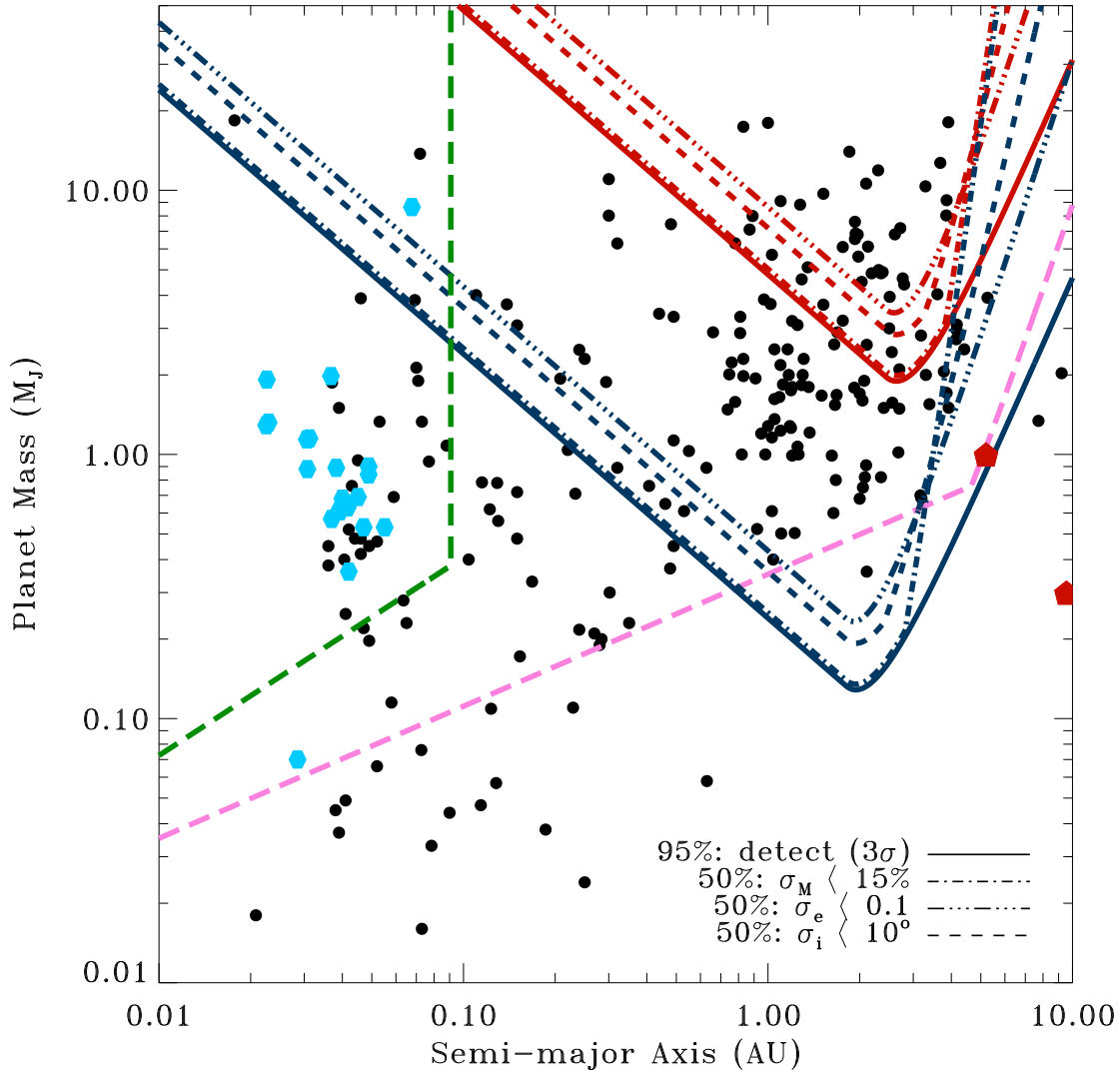


Fig. 22. Gaia discovery space for planets of given mass and orbital radius compared to the present-day sensitivity of other indirect detection methods, namely Doppler spectroscopy and transit photometry. Red curves of different styles have the same meaning as in Figure 21 assuming a $1-M_{\odot}$ G dwarf primary at 200 pc, while the blue curves are for a $0.5-M_{\odot}$ M dwarf at 25 pc. The radial velocity curve (pink line) is for detection at the $3\sigma_{RV}$ level, assuming $\sigma_{RV} = 3 \text{ m s}^{-1}$, $M_{\star} = 1 M_{\odot}$, and 10-yr survey duration. For transit photometry (green curve), the assumptions of Gaudi et al. (2005) are used, i.e. $\sigma_V = 5$ milli-mag, $S/N = 9$, $M_{\star} = 1 M_{\odot}$, $R_{\star} = 1 R_{\odot}$, uniform and dense (> 1000 datapoints) sampling. Black dots indicate the inventory of exoplanets as of September 2007. Transiting systems are shown as light-blue filled pentagons. Jupiter and Saturn are also shown as red pentagons.

mass and period distributions of exoplanets (see for example Butler et al. 2006), and by imposing that the fraction of planets with $1 \leq M_p \leq 15 M_J$ and $2 \leq P \leq 3000 \text{ d}$ equals the observed 7% for F-G-K normal stars with $-0.5 \leq [\text{Fe}/\text{H}] \leq 0.5$ (Marcy et al. 2005).

An estimate of the number of giant planets at a given distance d (in pc) whose astrometric signal could be detected by Gaia with 3σ confidence 95% of the time is then given by $N_d \sim 0.95 \times f_p \times N_{\star}$, where N_{\star} is computed within a sphere of radius d centered on the Sun for given limiting magnitude and spectral type, while the value of f_p is calculated integrating over a specific range of masses and periods. The number of planets for which, say, masses will be determined at least 50% of the time with an accuracy of better than 15% will instead be: $N_m \sim 0.50 \times N_d$. The results are summarized in Table 2. One then realizes that, based on our present knowledge of giant planets frequencies ($M_p > 1 - 3 M_J$), integrated over a wide range of spectral types and metallicities, Gaia could then find ~ 8000

such objects, and accurately measure masses and orbital parameters for ~ 4000 of them.

4.1.2. How many multiple-planet systems will Gaia find?

As of December 2007, 24 planet-bearing stars are orbited by more than one planet, corresponding to $\sim 12\%$ of the total sample of RV-detected systems⁴. However, many systems known to host one exoplanet show more distant, long-period, sub-stellar companions with highly significant but incomplete orbits (with inferred semi-major axis typically beyond 5 AU). Recent analyses of these long-term trends (Wright et al. 2007) indicate that $\sim 30\%$ of known exoplanet systems show significant evidence of

⁴ Johnson et al. (2007) and Setiawan et al. (2008) report possible multiple companions around GJ 317 and HD 47536. We elect not to include them as their orbits are either only loosely constrained or not yet statistically very significant

multiplicity. Considering that the mass distribution of planets increases steeply toward lower masses (e.g., Marcy et al. 2005), incompleteness must be considerable between 1.0 and 0.1 Jupiter-masses. Thus, the actual occurrence of multiple planets among stars having one known planet is likely considerably greater than 30%.

We report in Table 3 the relevant parameters of the multiple-planet systems with well-measured orbits known to-date, ordered by increasing distance of the system from the Sun. The expected values of the astrometric signature (α_{\min}) are computed assuming perfectly edge-on, coplanar configurations ($\sin i_j = 1$, for $j = 1, \dots, n_p$). The single-measurement precision is $\sigma_\psi = 8 \mu\text{as}$ for all stars. Of these systems, $\sim 50\%$ have more than one component with $\alpha_{\min} > 3\sigma_\psi$, $\sim 40\%$ have components with $\alpha_{\min} > 3\sigma_\psi$ as well as $P < 5 - 6$ yr, and some 16% have both $\alpha_{\min} > 10\sigma_\psi$ as well as $P < 5 - 6$ yr. Extrapolating from the numbers obtained in the previous Section and the ones above, one then infers that of the ~ 8000 new planetary systems discovered by Gaia, ~ 1000 would have multiplicity greater than one, and $\sim 400 - 500$ could have orbital parameters and masses measured to better than 15% – 20% accuracy.

Table 3. List of relevant parameters for known planetary systems.

Planet	d (pc)	M_{\star} (M_{\odot})	$M_p \sin i$ (M_J)	a (AU)	α (μ as)
GJ 876b	4.72	0.32	1.93	0.21	265.6
GJ 876c			0.56	0.13	48.0
GJ 876d			0.02	0.02	0.2
GJ 581b	6.26	0.31	0.05	0.04	1.0
GJ 581c			0.02	0.07	0.6
GJ 581d			0.02	0.25	3.1
HD 69830b	12.60	0.86	0.03	0.08	0.2
HD 69830c			0.04	0.19	0.7
HD 69830d			0.06	0.63	3.4
55 Cncb	13.40	1.03	0.78	0.11	6.7
55 Cncc			0.22	0.24	3.9
55 Cncd			3.92	5.26	1534.0
55 Cnce			0.05	0.04	0.1
ν Andb	13.47	1.27	0.69	0.06	2.4
ν Andc			1.98	0.83	95.1
ν Andd			3.95	2.51	575.3
47 Umab	13.97	1.03	2.60	2.11	376.7
47 Umac			1.34	7.73	347.5
HD 160691b	15.30	1.08	1.67	1.50	153.0
HD 160691c			3.10	4.17	781.1
HD 160691d			0.04	0.09	0.2
HD 160691e			0.52	0.92	29.1
HD 190360c	15.89	1.04	0.06	0.13	0.5
HD 190360b			1.50	3.92	365.7
HD 128311b	16.60	0.80	2.18	1.10	174.8
HD 128311c			3.21	1.76	415.1
HD 82943b	27.46	1.18	1.75	1.19	64.7
HD 82943c			2.01	0.75	46.6
HD 37124c	33.00	0.91	0.68	3.19	75.0
HD 37124b			0.61	0.53	11.1
HD 37124d			0.60	1.64	33.8
HD 11964b	33.98	1.13	0.11	0.23	0.7
HD 11964c			0.70	3.17	58.0
HD 169830b	36.32	1.40	2.88	0.81	46.0
HD 169830c			4.04	3.60	285.4
HD 217107b	37.00	1.02	1.33	0.07	2.6
HD 217107c			2.50	4.41	292.3
HD 12661b	37.16	1.07	2.30	0.83	47.6
HD 12661c			1.57	2.56	101.0
HD 168443b	37.88	1.06	8.02	0.30	59.8
HD 168443c			18.10	3.91	1314.1
HD 38529b	42.43	1.39	0.78	0.13	1.7
HD 38529c			12.70	3.68	789.4
HD 155358b	42.70	0.87	0.89	0.63	15.1
HD 155358c			0.50	1.22	16.6
HD 202206b	46.34	1.13	17.40	0.83	273.0
HD 202206c			2.44	2.55	117.9
HIP 14810b	52.90	0.99	3.84	0.07	5.1
HIP 14810c			0.76	0.41	5.9
HD 74156b	64.56	1.05	1.88	0.29	8.0
HD 74156d			0.4	1.04	6.1
HD 74156c			8.03	3.85	456.1
HD 108874c	68.50	1.00	1.02	2.68	39.9
HD 108874b			1.36	1.05	20.9
HD 73526b	99.00	1.02	2.90	0.66	18.6
HD 73526c			2.50	1.05	25.5

Table 4. Number of multiple-planet systems detected and measured by Gaia.

Case	Number of Systems
1) Detection	~ 1000
2) Orbits and masses to better than 15% – 20% accuracy	$\sim 400 - 500$
3) Successful coplanarity tests	~ 150

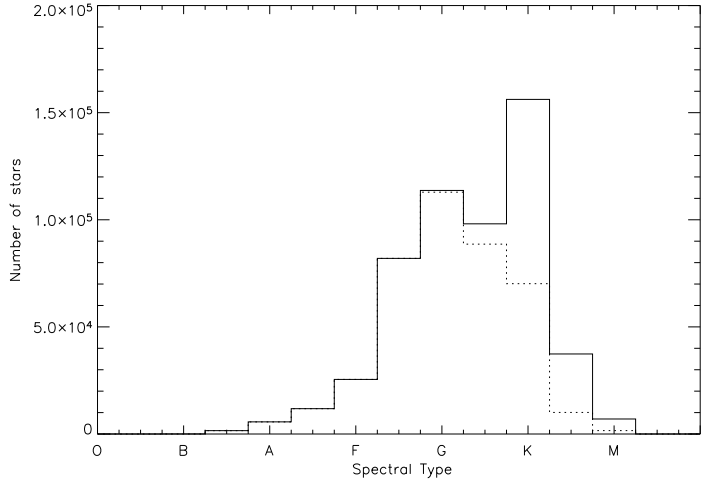
For some 150 systems with very favorable configurations, and enough redundancy in the number of observations, coplanarity tests could be performed, with expected uncertainties on the mutual inclination angle of $\sim 10^\circ$, or smaller. In terms of systems for which the Gaia data alone could provide reasonably good orbital solutions, this is about a twenty-fold improvement with respect to the present-day number of systems with well-determined orbits, and even the number of potential systems for which coplanarity analysis could be successfully carried out compares favorably to today's sample, presently populated by zero objects. These numbers are summarized in Table 4. Again, these results should be considered as lower limits, given the increasingly convincing evidence for a frequency of multiple-planet systems at least a factor of 2-3 greater than the value used here for the extrapolation.

4.2. The Gaia legacy

It is easy to realize how the statistical value of such large samples of newly detected giant planets and planetary systems would be instrumental for critical testing of planet formation and evolution models. To illustrate more clearly the wealth of information potentially contained in the data collected by Gaia, let us ask four fundamental questions for the astrophysics of planetary systems, and see how, based on the results presented in this paper, Gaia could help address them (complementing other datasets obtained with a variety of techniques).

4.2.1. How do planet properties and frequencies depend upon the characteristics of the parent stars?

Twelve years after the first discovery announcement (Mayor & Queloz 1995), the observational data on extrasolar planets are providing growing evidence that planetary systems properties (orbital elements and mass distributions, and correlations amongst them) and frequencies appear to depend upon the characteristics of the parent stars (spectral type, age, metallicity, binarity/multiplicity). Doppler surveys have begun in the recent past to put such trends on firmer statistical grounds. For example, dedicated surveys of metal-rich (Fischer et al. 2005; Bouchy et al. 2005) and metal-poor dwarfs (Sozzetti et al. 2006; Mayor et al. 2003⁵) are currently providing data to improve the statistical significance of the strong correlation between planet occurrence rates and stellar metallicity (e.g., Gonzalez 1997; Santos et al. 2004; Fischer & Valenti 2005). Similarly, other groups have been monitoring samples of bright M dwarfs (Butler et al. 2004; Bonfils et al. 2005; Endl et al. 2006; Johnson et al. 2007b, and

**Fig. 23.** Stellar content to $d < 200$ pc, as function of the spectral type, for $V < 13$ (solid line) and $V < 12$ (dotted line).

references therein), Hertzsprung gap sub-giants (Johnson et al. 2006, 2007a), heavily evolved stars belonging to the red-giant branch and clump regions of the H-R diagram (Frink et al. 2002; Setiawan et al. 2005; Sato et al. 2003; Hatzes et al. 2005; Lovis & Mayor 2007; Niedzielski et al. 2007, and references therein), early-type dwarfs (Galland et al. 2005), and relatively young stars (Setiawan et al. 2007a), in order to probe the possible dependence of f_p on stellar mass and age. However, the typical sample sizes of these surveys are of order of a few hundred objects, sufficient to test only the most outstanding difference between the various populations. It is thus desirable to be able to provide as large a database as possible of stars screened for planets.

As we have seen, the size of the stellar sample available for planet detection and measurement to the Gaia all-sky astrometric survey will be approximately a few hundred thousand relatively bright ($V < 13$) stars with a wide range of spectral types, metallicities, and ages out to ~ 200 pc. The sample-size is thus comparable to that of planned space-borne transit surveys, such as CoRoT and Kepler. The expected number of giant planets detected and measured (see Table 2) could be several thousands, depending on actual giant planet frequencies as a function of spectral type and orbital distance. This number is comparable to the size of the combined target lists of present-day ground-based Doppler surveys and of future astrometric projects such as VLTI/PRIMA and SIM. The Gaia unbiased and complete magnitude limited census of stars screened for new planets will allow, for example, to test the fine structure of giant planet parameters distributions and frequencies, and to investigate their possible changes as a function of stellar mass with unprecedented resolution. From Figure 23, of order of tens of thousands of normal stars in $0.1 M_\odot$ bins would become available for such investigations. Furthermore, the ranges of orbital parameters and giant planet host characteristics probed by the Gaia survey would crucially complement both transit observations (which strongly favor short orbital periods and are subject to stringent requisites on favorable orbital alignment), and radial-velocity measurements (which can be less effectively carried out for stars covering a wide range of spectral types, metallicities, and ages and do not allow to determine either the true planet mass or the full three-dimensional orbital geometry).

Thus, the ability to simultaneously and systematically determine planetary frequency and distribution of orbital parameters

⁵ <http://www.eso.org/observing/proposals/gto79/harps/4.txt>

for the stellar mix in the solar neighborhood without any potential biases induced by the choice of specific selection criteria for target lists, stems out as a fundamental contribution that Gaia will uniquely provide, the only limitations being those intrinsic to the mission, i.e., to the actual sensitivity of the Gaia measurements to planetary perturbations, which in this paper we have quantitatively gauged.

4.2.2. What is the preferred method of gas giant planet formation?

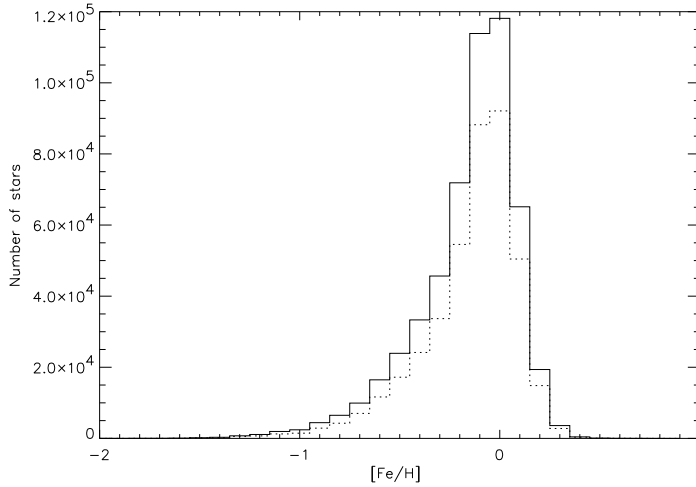


Fig. 24. Stellar distribution in the solar neighborhood ($d < 200$ pc) as function metallicity, for $V < 13$ (solid line) and $V < 12$ (dotted line).

The two main competing models of giant-planet formation by *core accretion* (e.g., Pollack et al. 1996. For a review see Lissauer & Stevenson 2007) and *disk instability* (e.g., Boss 2001. For a review see Durisen et al. 2007) make very different predictions regarding formation time-scales (Mayer et al. 2002; Alibert et al. 2005; Boss 2006), planet properties (Armitage et al. 2002; Kornet & Wolf 2006; Ida & Lin 2004a, 2005, 2008; Rice et al. 2003b), and frequencies as a function of host star characteristics (Laughlin et al. 2004; Ida & Lin 2004b, 2005, 2008; Kornet et al. 2005, 2006; Rice et al. 2003b; Boss 2000, 2002, 2006). Furthermore, correlations between orbital elements and masses, and possibly between the former and some of the host star characteristics (metallicity, mass) might reflect the outcome of a variety of migration processes and their possible dependence on environment (Livio & Pringle 2003; Ida & Lin 2004a, 2008; Boss 2005; Burkert & Ida 2007). Some of these predictions could be tested on firm statistical grounds by extending planet surveys to large samples of stars that are not readily accessible to Doppler surveys.

For example, Galaxy models (Bienaymé et al. 1987; Robin & Crézé 1986) predict ~ 4000 F–G–K dwarfs and sub-dwarfs to 200 pc, brighter than $V = 13$ mag, and with metallicity $[\text{Fe}/\text{H}] < -1.0$ (see Figure 24). The entire population will be screened by Gaia for giant planets on wide orbits thus complementing the shorter-period ground-based spectroscopic surveys (e.g., Sozzetti et al. 2006), which are also limited in the sample sizes due to the intrinsic faintness and weakness of the spectral lines of the targets. These data combined would allow for improved understanding of the behavior of the probability of planet formation in the low-metallicity regime, by direct comparison

between large samples of metal-poor and metal-rich stars, in turn putting stringent constraints on the proposed planet formation models and helping to better the role of stellar metallicity in the migration scenarios for gas giant planets.

Table 5. The closest (≤ 200 pc) star forming regions and young stellar kinematic groups.

Name	Distance (pc)	Age (Myr)
Hercules-Lyra	15-40	100
AB Doradus	20-50	30-50
Subgroup B4	20-50	80-100
β Pictoris	30-50	8-15
Tucana-Horologium	50-60	8-50
TW Hya	50	3-50
MBM 12	60-110	3-10
η Chamaeleontis	90-150	8-10
η Carinae	100	8
MBM 20	110-160	3-10
Pleades	125	75-100
ρ Ophiuchi	125-150	1-2
Taurus-Auriga	135	1-2
Corona Austrina	140	1-2
Lupus	140	1-2
o Velorum	160	30
θ Carinae	160	30
Scorpio-Centaurus	160-180	2-20
α Persei	175	85
Serpens	200	5-10

Furthermore, within the useful (for Gaia) distance horizon of ~ 200 pc, hundreds of relatively bright ($V < 13 - 14$) young stars can be found in some twenty or so nearby star-forming regions and young associations (see Table 5 for a list of young associations, open clusters, and moving groups in the age range $\sim 1 - 100$ Myr in the solar neighborhood, with ages in the approximate range 1-100 Myr. The data, ordered by increasing distance from the Sun, are from Zuckermann & Song (2004, and references therein) and López-Santiago et al. (2006, and references therein)). All these stars will be observed by Gaia with enough astrometric precision to detect the presence of massive giant planets ($M_p \gtrsim 2 M_J$) orbiting at 2-4 AU. The possibility to determine the epoch of giant planet formation in the protoplanetary disk would provide the definitive observational test to distinguish between the proposed theoretical models. These data would uniquely complement near- and mid-infrared imaging surveys (e.g., Burrows 2005, and references therein) for direct detection of young, bright, wide-separation ($a > 30 - 100$ AU) giant planets, such as JWST.

4.2.3. How do dynamical interactions affect the architecture of planetary systems?

The highly eccentric orbits of planetary systems have been explained so far calling into question a variety of dynamical mechanisms, such as interactions between a planet and the gaseous disk, planet-planet resonant interactions, close encounters between planets, secular interactions with a companion star (see for example Ford & Rasio 2007, and references therein). Some of these eccentricity excitation mechanisms can give rise to very different orbital architectures, including significantly non-coplanar orbits (Thommes & Lissauer 2003). An effective way to

understand their relative roles would involve measuring the mutual inclination angle between pairs of planetary orbits. Studies addressing the long-term dynamical stability issue for multiple-planet systems (presently divided in three broad classes of hierarchical, secularly interacting and resonantly interacting systems. See for example Kiseleva-Eggleton et al. 2002; Ji et al. 2003 and references therein; Correia et al. 2005; Barnes & Quinn 2004; Goździewski & Konacki 2004 and references therein), as well as the possibility of formation and survival of terrestrial planets in the Habitable Zone of the parent star (Menou & Tabachnik 2003; Jones et al. 2005 and references therein), would also greatly benefit from knowledge of the mutual inclination angle between planetary orbits.

The only way to provide meaningful estimates of the full three-dimensional geometry of *any* planetary system (without restrictions on the orbital alignment with respect to the line of sight) is through direct estimates of the mutual inclinations angles using high-precision astrometry. We have shown here how, extrapolating from today's knowledge of the frequency and architectures of multiple-planet systems, Gaia could detect and measure several hundred such systems, and perform a significant coplanarity analysis in a few hundred cases (see Table 4). These data, combined with those available from Doppler measurements and transit photometry and transit timing (e.g., Miralda Escudé 2002; Holman & Murray 2005; Agol et al. 2005), would then allow to put studies of the dynamical evolution of planetary systems on firmer grounds.

4.2.4. What are the phase functions and light curves of gas giant planets?

The combination of high-cadence, milli-mag photometric and $1\text{--}5\text{ m s}^{-1}$ precision radial-velocity measurements of transiting planet systems provides the fundamental observational data (planetary mass, radius, density, and gravity) needed for a meaningful comparison with structural models of hot Jupiters (e.g., Burrows 2005, and references therein). The special geometry of a transiting planet also permits a number of follow-up studies, which in particular have enabled direct observation of their transmission spectra and emitted radiation (Charbonneau et al. 2007, and references therein). These data provide the first observational constraints on atmospheric models of these extrasolar gas giants (Burrows 2005, and references therein).

The next logical step, the direct detection of extrasolar giant planets using high-contrast imaging instruments, requires that their dim light be separated from under the glare of their bright parent stars. Several theoretical studies (Hubbard et al. 2002; Baraffe et al. 2003; Sudarsky et al. 2005; Dyudina et al. 2005; Burrows et al. 2004, 2007) have discussed exoplanet apparent brightness in reflected host star light (expressed in units of the planet/host star flux ratio $\log(F_{\text{pl}}/F_{\text{star}})$ as functions of orbit geometry, orbital phase, cloud cover, cloud composition, mass and age. In particular, orbit and orientation of an extrasolar planet play a crucially important role in its flux at the Earth and in its interpretation, with strong dependence on eccentricity and inclination (Burrows et al. 2004). Depending upon e and i , $\log(F_{\text{pl}}/F_{\text{star}})$ can be essentially constant (in case of $e \approx 0.0$, $i \approx 0^\circ$, for example), or vary by over an order of magnitude (in case of $e \approx 0.6$, $i \approx 90^\circ$ for example) along the orbit of an exoplanet, and this can induce significant changes in the chemical composition of its atmosphere (e.g., from cloudy to cloud-free). As for the knowledge of the actual mass of the planet, particularly at young ages theory predicts changes in intrinsic luminos-

ity by a factor of nearly 100 can occur between objects in the mass range $1 M_J \lesssim M_p \lesssim 5 M_J$. The few wide-separation substellar companions detected to-date by means of direct imaging techniques (Chauvin et al. 2005a, 2005b; Neuhauser et al. 2005; Biller et al. 2006), have planetary-mass solutions within their error bars, but these mass estimates rely upon so far poorly calibrated theoretical mass-luminosity relationships, thus their actual nature (planets or brown dwarfs) remains highly uncertain. It is then clear how accurate knowledge of all orbital parameters and actual mass are essential for understanding the thermophysical conditions on a planet and determining its visibility. Recently, the first prediction of epoch and location of maximum brightness was derived for the giant planet orbiting ϵ Eridani using HST/FGS astrometry in combination with high-precision radial-velocities (Benedict et al. 2006). As of today, there are some 20 RV-detected exoplanets with $M_p \sin i > 1 M_J$, $P > 1$ yr and projected separations > 0.1 arcsec (the typical size of the Inner Working Angle of coronagraphic instruments presently under study) for which Gaia could provide information on where and when to observe, and presumably several tens more will be discovered in the next several years by Doppler surveys and by Gaia itself. Gaia's ability to accurately measure orbital parameters (including inclination) and actual mass of a planet through high-precision astrometric measurements would then provide important supplementary data to aid in the interpretation of direct detections of exoplanets.

4.2.5. How common are the terrestrial planets?

With the advent of the new generation of ultra-high precision spectrographs such as HARPS (e.g., Pepe et al. 2004), radial-velocity programs achieving $\lesssim 1\text{ m s}^{-1}$ measurement precision have begun detecting around nearby M dwarfs close-in planets with $M_p \sin i \approx 5\text{--}10 M_\oplus$ (Rivera et al. 2005; Lovis et al. 2006; Udry et al. 2007), so-called 'super-Earths', likely to be mostly 'rocky' in composition. One of them, GJ 581d (Udry et al. 2007), may orbit within the Habitable Zone of the parent star, depending on the assumed exoplanet atmosphere (Selsis et al. 2007; von Bloh et al. 2007). The announcement of the discovery of a short-period habitable terrestrial planet around a low-mass star might well be just around the corner. However, the strongest statistical constraints (including bona-fide detections) on the frequency of Earth-sized habitable planets orbiting Sun-like stars will likely come from currently operating and upcoming space-borne observatories devoted to ultra-high precision transit photometry, such as CoRoT (Baglin et al. 2002) and Kepler (Borucki et al. 2003), and very high-precision narrow-angle astrometry, such as SIM (Beichman et al., 2007, and references therein).

The next challenging step will be to directly detect and characterize terrestrial, habitable planets orbiting stars very close ($d \lesssim 25$ pc) to our Sun, searching for elements in their atmospheres that can be interpreted as 'bio-markers' (Hitchcock & Lovelock 1967; Des Marais et al. 2002; Seager et al. 2005; Tinetti et al. 2007; Kaltenegger et al. 2007), implying the likely existence of a complex biology on the surface. Imaging terrestrial planets is presently the primary science goal of the coronagraphic and interferometric configurations of the Terrestrial Planet Finder (TPF-C & TPF-I) and Darwin missions (Beichman et al. 2007, and references therein). Ultimately, the final list of targets will be formulated taking into account constraints coming from the knowledge of f_p in the terrestrial mass regime, potential stellar host characteristics (spectral type, binarity, surface activity), and environment. In this respect, Gaia astrometry of all nearby stars, including the large numbers of M dwarfs,

within 25 pc from the Sun will be an essential ingredient in order to provide Darwin/TPF with a comprehensive database of F-G-K-M stars with and without detected giant planets orbiting out to several AUs from which to choose additional targets based on the presence or absence of Jupiter signposts (Sozzetti et al. 2003b). Such measurements will uniquely complement ongoing and planned radial-velocity programs and exo-zodiacal dust emission observations from the ground with Keck-I, LBTI, and VLTI.

5. Summary and conclusions

We have presented results from an extensive program of double-blind tests for planet detection and measurement with Gaia. The main findings obtained in this study include: a) an improved, more realistic assessment of the detectability and measurability of single and multiple planets under a variety of conditions, parametrized by the sensitivity of Gaia, and b) an assessment of the impact of Gaia in critical areas of planet research, in dependence on its expected capabilities.

Overall, the results of our earlier works (Lattanzi et al. 2000a; Sozzetti et al. 2001, 2003a) are essentially confirmed, with a fundamental improvement due to the successful development of independent orbital fitting algorithms applicable to real-life data that do not utilize any a priori knowledge of the orbital parameters of the planets. In particular, the results of the T1 test (planet detection) indicate that planets down to astrometric signatures $\alpha \approx 25 \mu\text{as}$, corresponding to ~ 3 times the assumed single-measurement error, can be detected reliably and consistently, with a very small number of false positives (depending on the specific choice of the threshold for detection).

The results of the T2 test (single-planet orbital solutions) indicate that: 1) orbital periods can be retrieved with very good accuracy (better than 10%) and small bias in the range $0.3 \leq P \leq 6$ yrs, and in this period range the other orbital parameters and the planet mass are similarly well estimated. The quality of the solutions degrades quickly for periods longer than the mission duration, and in particular the fitted value of P is systematically underestimated; 2) uncertainties in orbit parameters are well understood; 3) nominal uncertainties obtained from the fitting procedure are a good estimate of the actual errors in the orbit reconstruction. Modest discrepancies between estimated and actual errors arise only for planets with extremely good signal (errors are overestimated) and for planets with very long period (errors are underestimated); such discrepancies are of interest mainly for a detailed numerical analysis, but they do not touch significantly the assessment of Gaia's ability to find planets and our preparedness for the analysis of perturbation data.

The results of the T3 test (multiple-planet orbital solutions) indicate that 1) over 70% of the simulated orbits under the conditions of the T3 test (for every two-planet system, periods shorter than 9 years and differing by at least a factor of two, $2 \leq \alpha/\sigma_\psi \leq 50$, $e \leq 0.6$) are correctly identified; 2) favorable orbital configurations (both planet with periods ≤ 4 yr and astrometric signal-to-noise ratio $\alpha/\sigma_\psi \geq 10$, redundancy of over a factor of 2 in the number of observations) have periods measured to better than 10% accuracy > 90% of the time, and comparable results hold for other orbital elements; 3) for these favorable cases, only a modest degradation of up to 10% in the fraction of well-measured orbits is observed with respect to single-planet solutions with comparable properties; 4) the overall results are mostly insensitive to the mutual inclination of pairs of planetary orbits; 5) over 80% of the favorable configurations have i_{rel} mea-

sured to better than 10° accuracy, with only mild dependencies on its actual value, or on the inclination angle with respect to the line of sight of the planets; 6) error estimates are generally accurate, particularly for fitted parameters, while modest discrepancies (errors are systematically underestimated) arise between formal and actual errors on i_{rel} .

Then, we attempted to put Gaia's potential for planet detection and measurement in context, by identifying several areas of planetary science in which Gaia can be expected, on the basis of our results, to have a dominant impact, and by delineating a number of recommended research programs that can be conducted successfully by the mission as planned. In conclusion, Gaia's main strength continues to be the unbiased and complete magnitude limited census of stars of all ages, spectral types, and metallicity in the solar neighborhood that will be screened for new planets, which translates into the ability to measure actual masses and orbital parameters for possibly thousands of planetary systems.

The Gaia data have the potential to a) significantly refine our understanding of the statistical properties of extrasolar planets: the predicted database of several thousand extrasolar planets with well-measured properties will allow for example to test the fine structure of giant planet parameters distributions and frequencies, and to investigate their possible changes as a function of stellar mass with unprecedented resolution; b) help crucially test theoretical models of gas giant planet formation and migration: for example, specific predictions on formation time-scales and the role of varying metal content in the protoplanetary disk will be probed with unprecedented statistics thanks to the thousands of metal-poor stars and hundreds of young stars screened for giant planets out to a few AUs; c) improve our comprehension of the role of dynamical interactions in the early as well as long-term evolution of planetary systems: for example, the measurement of orbital parameters for hundreds of multiple-planet systems, including meaningful coplanarity tests will allow to discriminate between various proposed mechanisms for eccentricity excitation; d) aid in the understanding of direct detections of giant extrasolar planets: for example, actual mass estimates and full orbital geometry determination (including inclination angles) for suitable systems will inform direct imaging surveys about where and when to point, in order to estimate optimal visibility, and will help in the modeling and interpretation of giant giant planets' phase functions and light curves; e) provide important supplementary data for the optimization of the selection of targets for Darwin/TPF: for example, all F-G-K-M stars within the useful volume (~ 25 pc) will be screened for Jupiter- and Saturn-sized planets out to several AUs, and these data will help to probe the long-term dynamical stability of their Habitable Zones, where terrestrial planets may have formed, and maybe found.

We conclude by providing a word of caution, in light of the possible degradations in the expected Gaia astrometric precision on bright stars ($V < 13$). Indeed, refinements in the overall Gaia error model (which includes centroiding as well as systematic uncertainties due to a variety of calibration errors) are still possible, and a better understanding of some of the many effects that need to be taken into account may help reduce the present-day end-of-mission scientific contingency margin of $\sim 20\%$ which is included to account for discrepancies that may occur between the simplified error-budget assessment performed now and the true performances on real data. However, if ultimately a degradation of 35%–40% in the single-measurement precision on bright stars were to be confirmed, the Gaia science case for exoplanets would be affected to some degree of relevance. For example, by

Table 6. Number of single- and multiple-planet systems detected and measured by Gaia as a function of σ_ψ .

σ_ψ^a (μas)	N_\star^b	N_d^c	N_m^d	$N_{d,\text{mult}}^e$	$N_{m,\text{mult}}^f$	N_{copl}^g
8	500 000	8 000	4 000	1 000	500	159
12	148 148	2 370	1 185	296	148	47
16	62 500	1 000	500	125	62	19
24	18 519	296	148	37	18	5
40	4 000	64	32	8	4	1
80	500	8	4	1	0	0

^a Single-measurement precision^b Number of stars within the useful distance, assumed to scale with the cube of the radius (in pc) of a sphere centered around the Sun^c Number of single-planet systems detected^d Number of single-planet systems whose astrometric orbits are measured to better than 15% accuracy^e Number of multiple-planet systems detected^f Number of multiple-planet systems with orbits measured to better than 15%-20% accuracy^g number of multiple-planet systems for which successful coplanarity tests (with i_{rel} known to better than 10° accuracy) can be carried out.

simply scaling with the value of the astrometric signal needed for detection and measurement of the orbital parameters to 15%-20% ($\alpha/\sigma_\psi \sim 3 - 5$, see Figure 21), as σ_ψ increases the same type of system (same stellar mass, same planet mass, same orbital period) would be characterized at increasingly shorter distances. A comparison between numbers of detectable and measurable single- and multiple-planet systems as a function of increasing Gaia single-measurement error is presented in Table 6. Assuming that the number of objects scales with the cube of the radius (in pc) of a sphere centered around the Sun (with no distinction of spectral types), if σ_ψ degrades from $8 \mu\text{as}$ to $12 \mu\text{as}$ (closer to the present-day estimate) then this would correspond to a reduction of a factor ~ 2 in the distance limit and in a corresponding decrease in the number of stars available for investigation from $\sim 5 \times 10^5$ to $\sim 1.5 \times 10^5$. If σ_ψ were to worsen by a factor 2, the number of stars available for planet detection and measurement ($\sim 6 \times 10^4$) would be reduced by about an order of magnitude. Accordingly, the expected numbers of giant planets detected and measured would decrease from ~ 4000 to ~ 1200 and ~ 500 , respectively, and the number of multiple systems for which coplanarity could be established would diminish from ~ 160 to ~ 50 and ~ 20 , respectively. We conclude that a factor 2 degradation in astrometric precision would severely impact most of Gaia exoplanet science case. We are aware that, instead of using simple scaling laws, one should provide more quantitative statements based on new simulations. However, this activity will necessarily be tied to further developments of the understanding of the technical specifications of Gaia and its instruments, and of its observation and data analysis process; therefore, we plan to revisit these issues as needed in the future, depending on the actual evolution of the knowledge of the Gaia measurement process.

Acknowledgements. We are indebted to an anonymous referee for a very careful, critical reading of the manuscript, and many useful comments and suggestions which helped to greatly improve it. This research has made use of NASA's Astrophysics Data System Abstract Service and of the SIMBAD database, operated at CDS, Strasbourg, France. M.G.L. acknowledges support from STScI through the Institute's Visitor Program for 2007. We gratefully acknowledge INAF (P. Vettolani, Projects Department) for its continued support of the Italian participation to the Gaia mission.

References

- Agol, E., Steffen, J., Sari, R., & Clarkson, W. 2005, MNRAS, 359, 567
- Alibert, Y., Mordasini, C., Benz, W., & Winisdoerffer, C. 2005, A&A, 434, 343
- Armitage, P. J., Livio, M., Lubow, S. H., & Pringle, J. E. 2002, MNRAS, 334, 248
- Bakos, G. Á., et al. 2007, ApJ, 671, L173
- Baglin, A., et al. 2002, in Radial and Nonradial Pulsations as Probes of Stellar Physics, eds. C. Aerts, T. R. Bedding, & J. Christensen-Dalsgaard, ASP Conf. Ser., 259, 626
- Baraffe, I., Chabrier, G., Allard, F., Hauschildt, P.H. 2003, A&A, 402, 701
- Barnes, R., & Quinn, T. 2004, ApJ, 611, 494
- Bean, J. L., et al. 2007, AJ, 134, 749
- Beaulieu, J.-Ph., et al. 2006, Nature, 439, 437
- Beichman, C. A., Fridlund, M., Traub, W. A., Stapelfeldt, K. R., Quirrenbach, A., & Seager, S. 2007, in Protostars and Planets V, B. Reipurth, D. Jewitt, and K. Keil (eds.), University of Arizona Press, Tucson, 915
- Benedict, G. F., et al. 2002, ApJ, 581, L115
- Benedict, G. F., et al., 2006, AJ, 132, 2206
- Bienaymé, O., Robin, A. C., & Crézé, M. 1987, A&A, 180, 94
- Billar, B. A., Kasper, M., Close, L. M., Brandner, W., & Kellner, S. 2006, ApJ, 641, L141
- Bond, I., et al., 2004, ApJ, 606, L155
- Bonfils, X., et al. 2005, A&A, 443, L15
- Borucki, W. J., et al. 2003, in Future EUV/UV and Visible Space Astrophysics Missions and Instrumentation, eds. J. C. Blades & O. H. W. Siegmund, Proc. SPIE, 4854, 129
- Boss, A. P. 2000, ApJ, 536, L101
- Boss, A. P. 2001, ApJ, 563, 367
- Boss, A. P. 2002, ApJ, 567, L149
- Boss, A. P. 2005, ApJ, 629, 535
- Boss, A. P. 2006, ApJ, 643, 501
- Bouchy, F., Pont, F., Santos, N. C., Melo, C., Mayor, M., Queloz, D., & Udry, S. 2004, A&A, 421, L13
- Bouchy, F., et al. 2005, A&A, 444, L15
- Burkert, A., & Ida, S. 2007, ApJ, 660, 845
- Burrows, A., Sudarsky, D., & Hubeny, I. 2004, ApJ, 609, 407
- Burrows, A. 2005, Nature, 433, 261
- Burrows, A., Budaj, J., & Hubeny, I. 2007, ApJ, accepted (arXiv:0709.4080)
- Butler, R. P., Vogt, S. S., Marcy, G. W., Fischer, D. A., Wright, J. T., Henry, G. W., Laughlin, G., & Lissauer, J. J. 2004, ApJ, 617, 580
- Butler, R. P., et al. 2006, ApJ, 646, 505
- Casertano, S., Lattanzi, M. G., Perryman, M. A. C., & Spagna, A. 1996, Ap&SS, 241, 89
- Casertano, S., & Sozzetti, A. 1999, in Working on the Fringe: Optical and IR Interferometry from Ground and Space, ed. S. Unwin & R. Stachnik, ASP Conf. Ser. 194, 171
- Catanzarite, J., Shao, M., Tanner, A., Unwin, S., & Yu, J. 2006, PASP, 118, 1319
- Charbonneau, D., Brown, T. M., Burrows, A., & Laughlin, G. 2007, in Protostars and Planets V, B. Reipurth, D. Jewitt, and K. Keil (eds.), University of Arizona Press, Tucson, 701
- Chauvin, G., et al. 2005a, A&A, 438, L25
- Chauvin, G., et al. 2005b, A&A, 438, L29
- Collier Cameron, A., et al. 2006, MNRAS, 375, 95
- Correia, A. C. M., Udry, S., Mayor, M., Laskar, J., Naef, D., Pepe, F., Queloz, D., & Santos, N. C. 2005, A&A, 440, 751
- de Felice, F., Lattanzi, M. G., Vecchiato, A., & Bernacca, P. L. 1998, A&A, 332, 1133
- de Felice, F., Bucciarelli, B., Lattanzi, M. G., & Vecchiato, A. 2001, A&A, 373, 336
- de Felice, F., Crosta, M. T., Vecchiato, A., Lattanzi, M. G., & Bucciarelli, B. 2004, ApJ, 607, 580
- Delplancke, F., et al. 2006, in Advances in Stellar Interferometry, eds. J.D. Monnier, M. Schöller, & W.C. Danchi, Proc. SPIE, 6268, 27
- Des Marais, D. J., et al. 2002, Astrobiology, 2, 153
- Durisen, R. H., Boss, A. P., Mayer, L., Nelson, A. F., Quinn, T., & Rice, W. K. M. 2007, in Protostars and Planets V, B. Reipurth, D. Jewitt, and K. Keil (eds.), University of Arizona Press, Tucson, 607
- Dyudina, U. A., Sackett, P. D., Bayliss, D. D. R., Seager, S., Porco, C. C., Throop, H. B., & Dones, L. 2005, ApJ, 618, 973
- Endl, M., Cochran, W. D., Kürster, M., Paulson, D. B., Wittenmyer, R. A., MacQueen, P. J., & Tull, R. G. 2006, ApJ, 649, 436
- Eriksson, U., & Lindegren, L. 2007, A&A, 476, 1389
- ESA 1997, The Hipparcos and Tycho Catalogues, ESA SP-1200
- Fischer, D. A., & Valenti, J. 2005, ApJ, 622, 1102
- Fischer, D. A., et al. 2005, ApJ, 620, 481
- Ford, E. B., & Tremaine, S. 2003, PASP, 115, 1171
- Ford, E. B. 2004, PASP, 116, 1083

- Ford, E. B. 2006, *PASP*, 118, 364
- Ford, E. B., & Gregory, P. C. 2007, in *Statistical Challenges in Modern Astronomy IV*, G.J. Babu and E.D. Feigelson (eds.), *ASP Conf. Ser.*, 371, 189
- Ford, E. B., & Rasio, F. A. 2007, *ApJ*, submitted (astro-ph/0703163)
- Frink, S., Mitchell, D. S., Quirrenbach, A., Fischer, D. A., Marcy, G. W., & Butler, R. P. 2002, *ApJ*, 576, 478
- Galland, F., Lagrange, A.-M., Udry, S., Chelli, A., Pepe, F., Beuzit, J.-L., & Mayor, M. 2005, *A&A*, 444, L21
- Gaudi, B. S., Seager, S., & Mallén-Omelas, G. 2005, *ApJ*, 623, 472
- Gonzalez G., 1997, *MNRAS*, 285, 403
- Gould, A., et al. 2006, *ApJ*, 644, L37
- Goździewski, K., & Konacki, M. 2004, *ApJ*, 610, 1093
- Green, R. M. 1985, *Spherical Astronomy*, Cambridge University Press
- Hatzes, A. P., Guenther, E. W., Endl, M., Cochran, W. D., Dillinger, M. P., & Bedalov, A. 2005, *A&A*, 437, 743
- Hitchcock, D. R., & Lovelock, J. E. 1967, *Icarus*, 7, 149
- Holman, M. J., & Murray, N. W. 2005, *Science*, 307, 1288
- Horne, J. H., & Baliunas, S. L. 1986, *ApJ*, 302, 757
- Hubbard, W. B., Burrows, A., & Lunine, J. I. 2002, *ARA&A*, 40, 103
- Ida, S., & Lin, D. N. C. 2004a, *ApJ*, 604, 388
- Ida, S., & Lin, D. N. C. 2004b, *ApJ*, 616, 567
- Ida, S., & Lin, D. N. C. 2005, *ApJ*, 626, 1045
- Ida, S., & Lin, D. N. C. 2008, *ApJ*, 673, 487
- Johnson, J. A., Marcy, G. W., Fischer, D. A., Henry, G. W., Wright, J. T., Isaacson, H., & McCarthy, C. 2006, *ApJ*, 652, 1724
- Johnson, J. A., et al. 2007a, *ApJ*, 655, 785
- Johnson, J. A., Butler, R. P., Marcy, G. W., Fischer, D. A., Vogt, S. S., Wright, J. T., & Peek, K. M. G. 2007b, *ApJ*, 670, 833
- Ji, J., Liu, L., Kinoshita, H., Zhou, J., Nakai, H., & Li, G. 2003, *ApJ*, 591, L57
- Jones, B. W., Underwood, D. R., & Sleep, P. N. 2005, *ApJ*, 622, 1091
- Kaltenegger, L., Traub, W. A., & Jucks, K. W. 2007, *ApJ*, 658, 598
- Kasting, J. F., Whitmire, D. P., & Reynolds, R. T. 1993, *Icarus*, 101, 108
- Kiseleva-Eggleton, L., Bois, E., Rambaux, N., & Dvorak, R. 2002, *ApJ*, 578, L145
- Klioner, S. A., & Kopeikin, S. M. 1992, *AJ*, 104, 897
- Klioner, S. A. 2003, *AJ*, 125, 1580
- Klioner, S. A. 2004, *Phys. Rev. D*, 69, No. 124001
- Konacki, M., Maciejewski, A. J., & Wolszczan, A. 2002, *ApJ*, 567, 566
- Konacki, M., Torres, G., Jha, S., & Sasselov, D. D. 2003, *Nature*, 421, 507
- Konacki, M., Torres, G., Sasselov, D. D., & Jha, S. 2005, *ApJ*, 624, 372
- Kornet, K., & Wolf, S. 2005, *A&A*, 454, 989
- Kornet, K., Bodenheimer, P., Różycka, M., & Stepinski, T. F. 2005, *A&A*, 430, 1133
- Kornet, K., Bodenheimer, P., & Różycka, M. 2006, *A&A*, 458, 661
- Kovács, G., et al. 2007, *ApJ*, 670, L41
- Lattanzi, M. G., Spagna, A., Sozzetti, A., & Casertano, S. 1997, in *Proc. of the ESA Symposium 'Hipparcos - Venice '97'*, ESA SP-402, 755
- Lattanzi, M. G., Spagna, A., Sozzetti, A., & Casertano, S. 2000a, *MNRAS*, 317, 211
- Lattanzi, M. G., Sozzetti, A., & Spagna, A. 2000b, in *From Extra-solar Planets to Cosmology: The VLT Opening Symposium*, ed. J. Bergeron & A. Renzini (Berlin: Springer-Verlag), 479
- Lattanzi, M. G., Casertano, S., Sozzetti, A., & Spagna, A. 2002, in *GAIA: A European Space Project*, eds. O. Bienaymé & C. Turon, *EAS Publications Series (EDP Sciences)*, 2, 207
- Lattanzi, M. G., Casertano, S., Jancart, S., Morbidelli, R., Pannunzio, R., Pourbaix, D., Sozzetti, A., & Spagna, A. 2005, in *The Three-Dimensional Universe with Gaia*, eds. C. Turon, K.S. O'Flaherty, & M.A.C. Perryman, *ESA SP-576*, 251
- Laughlin, G., Bodenheimer, P., & Adams, F. C. 2004, *ApJ*, 612, L73
- Laughlin, G., Butler, R. P., Fischer, D. A., Marcy, G. W., Vogt, S. S., & Wolf, A. S. 2005, *ApJ*, 622, 1182
- Lindgren, L., & de Bruijne, J. H. J. 2005, in *Astrometry in the Age of the Next Generation of Large Telescopes*, *ASP Conf. Ser.* 338, 25
- Lissauer, J. J., & Stevenson, D. J. 2007, in *Protostars and Planets V*, B. Reipurth, D. Jewitt, and K. Keil (eds.), University of Arizona Press, Tucson, 591
- Livio, M., & Pringle, J. E. 2003, *MNRAS*, 346, L42
- Lovis, C., et al. 2006, *Nature*, 441, 305
- Lovis, C., & Mayor, M. 2007, *A&A*, 472, 657
- López-Santiago, J., Montes, D., Crespo-Chacón, I., & Fernández-Figueroa, M. J. 2006, *ApJ*, 643, 1160
- Mandushev, G., et al. 2007, *ApJ*, 667, L195
- Marcy, G. W., Butler, R. P., Fischer, D. A., Vogt, S. S., Wright, J. T., Tinney, C. G., & Jones, H. R. A. 2005, *Progress of Theoretical Physics Supplement*, 158, 24
- Mayer L., Quinn T., Wadsley J., & Stadel J., 2002, *Science*, 298, 1756
- Mayor, M., & Queloz, D. 1995, *Nature*, 378, 355
- McArthur, B. E., et al. 2004, *ApJ*, 614, L81
- Menou, C., & Tabachnik, S. 2003, *ApJ*, 583, 473
- Miralda-Escudé, J. 2002, *ApJ*, 564, 1019
- Neuhäuser, R., Guenther, E. W., Wuchterl, G., Mugrauer, M., Bedalov, A., & Hauschildt, P. H. 2005, *A&A*, 435, L13
- Niedzielski, A., et al. 2007, *ApJ*, 669, 1354
- Pepe, F., et al. 2004, *A&A*, 423, 385
- Perryman, M. A. C., et al. 1997, *A&A*, 323, L49
- Perryman, M. A. C., et al. 2001, *A&A*, 369, 339
- Pollack, J. B., Hubickyj, O., Bodenheimer, P., Lissauer, J. J., Podolack, M., & Greenzweig, Y. 1996, *Icarus*, 124, 62
- Pont, F., Bouchy, F., Queloz, D., Santos, N. C., Melo, C., Mayor, M., & Udry, S. 2004, *A&A*, 426, L15
- Pont, F., et al. 2007, *A&A*, submitted (arXiv:0710.5278)
- Pourbaix, D. 2002, *A&A*, 385, 686
- Rice, W. K. M., Armitage, P. J., Bate, M. R., & Bonnell, I. A. 2003a, *MNRAS*, 338, 227
- Rice, W. K. M., Armitage, P. J., Bonnell, I. A., Bate, M. R., Jeffers, S. V., & Vine, S. G. 2003b, *MNRAS*, 346, L36
- Rivera, E., Lissauer, J. J., Butler, R. P., Marcy, G. W., Vogt, S. S., Fischer, D. A., Brown, T., Laughlin, G., & Henry, G. W. 2005, *ApJ*, 634, 625
- Robin, A. C., & Crézé, M. 1986, *A&A*, 157, 71
- Santos, N. C., Israelian, G., & Mayor, M. 2004, *A&A*, 415, 1153
- Sato, B., et al. 2003, *ApJ*, 597, L157
- Seager, S., Turner, E. L., Schafer, J., & Ford, E. B. 2005, *Astrobiology*, 5, 372
- Selsis, F., Kasting, J. F., Levrard, B., Paillet, J., Ribas, I., & Delfosse, X. 2007, *A&A*, 476, 1373
- Setiawan, J., Rodmann, J., da Silva, L., Hatzes, A. P., Pasquini, L., von der Lühe, O., de Medeiros, J. R., Döllinger, M. P., & Girardi, L. 2005, *A&A*, 437, L31
- Setiawan, J., Weise, P., Henning, Th., Launhardt, R., Miller, A., & Rodmann, J. 2007a, *ApJ*, 660, L145
- Setiawan, J., et al. 2008, in *Proceedings of the ESO Workshop "Precision Spectroscopy in Astrophysics"*, eds. L. Pasquini, M. Romaniello, N.C. Santos, & A. Correia, 201
- Sozzetti, A., Casertano, S., Lattanzi, M. G., & Spagna A. 2001, *A&A*, 373, L21
- Sozzetti, A., Casertano, S., Brown, R. A., & Lattanzi, M. G. 2002, *PASP*, 114, 1173
- Sozzetti, A., Casertano, S., Lattanzi, M. G., & Spagna A. 2003a, in *Towards Other Earths: DARWIN/TPF and the Search for Extrasolar Terrestrial Planets*, eds. M. Fridlund & T. Henning, *ESA SP-539*, 605
- Sozzetti, A., Casertano, S., Brown, R. A., & Lattanzi, M. G. 2003b, *PASP*, 115, 1072
- Sozzetti, A. 2005, *PASP*, 117, 1021
- Sozzetti, A., Torres, G., Latham, D. W., Carney, B. W., Stefanik, R. P., Boss, A. P., Laird, J. B., & Korzennik, S. G. 2006, *ApJ*, 649, 428
- Sudarsky, D., Burrows, A., Hubeny, I., & Li, A. 2005, *ApJ*, 627, 520
- Tabachnik, S., & Tremaine, S. 2002, *MNRAS*, 335, 151
- Takeuchi, T., Velusamy, T., & Lin, D. N. C. 2005, *ApJ*, 618, 987
- Tinetti, G., Rashby, S., & Yung, Y. L. 2007, *ApJ*, 644, L129
- Thommes, E. W., & Lissauer, J. J. 2003, *ApJ*, 597, 566
- Udalski, A., et al. 2005, *ApJ*, 628, L109
- Udalski, A., et al. 2007, *A&A*, submitted (arXiv:0711.3978)
- Udry, S., et al., 2007, *A&A*, 469, L43
- Unwin, S. C., et al. 2007, *PASP*, submitted (arXiv:0708.3953)
- Vecchiato, A., Lattanzi, M. G., Bucciarelli, B., Crosta, M., de Felice, F., & Gai, M. 2003, *A&A*, 399, 337
- von Bloh, W., Bounama, C., Cuntz, M., & Franck, S. 2007, *A&A*, 476, 1365
- Wright, J. T., et al. 2007, *ApJ*, 657, 533
- Zuckerman, B., & Song, I. 2004, *ARA&A*, 42, 685

Appendix A: The Simulated Model

The code for the generation of synthetic Gaia observations of planetary systems is run by the Simulators group.

We start by generating spheres of N targets. Each target's two-dimensional position is described in the ecliptic reference frame via a set of two coordinates λ_b and β_b , called here barycentric coordinates. We linearly update the barycentric position as a function of time, accounting for the (secular) effects of proper motion (two components, μ_λ and μ_β), the (periodic) effect of the parallax π , and the (Keplerian) gravitational perturbations induced on the parent star by one or more orbiting planets (mutual interactions between planets are presently not taken into account). The model of motion can thus be expressed as follows:

$$\mathbf{x}_{\text{ecl}} = \mathbf{x}_{\text{ecl}}^0 + \mathbf{x}_{\text{ecl}}^{\pi, \mu} + \sum_{j=1}^{n_p} \mathbf{x}_{\text{ecl}}^{\text{K}, j} \quad (\text{A.1})$$

Where:

$$\mathbf{x}_{\text{ecl}}^0 = \begin{pmatrix} \cos \beta_b \cos \lambda_b \\ \cos \beta_b \sin \lambda_b \\ \sin \beta_b \end{pmatrix}$$

is the initial position vector of the system barycenter. The various perturbative effects are initially defined in the tangent plane. The parallax and proper motion terms are contribute as:

$$\mathbf{x}_{\pi, \mu} = \begin{pmatrix} \mu_\lambda t + \pi F_\lambda \\ \mu_\beta t + \pi F_\beta \\ 0 \end{pmatrix}$$

Where the parallax factors are defined utilizing the classic formulation by Green (1985):

$$F_\lambda = -\sin(\lambda_b - \lambda_\odot)$$

$$F_\beta = -\sin \beta_b \sin(\lambda_b - \lambda_\odot)$$

and λ_\odot is the sun's longitude at the given time t . The term describing the Keplerian motion of the j -th planet in the tangent plane is:

$$\mathbf{x}_{\text{K}, j} = \begin{pmatrix} x_{\text{K}, j} \\ y_{\text{K}, j} \\ 0 \end{pmatrix} = \begin{pmatrix} \varrho_j \cos \vartheta_j \\ \varrho_j \sin \vartheta_j \\ 0 \end{pmatrix},$$

where ϱ_j is the separation and ϑ_j the position angle. The two coordinates $x_{\text{K}, j}$ and $y_{\text{K}, j}$ are functions of the 7 orbital elements:

$$x_{\text{K}, j} = a_j(1 - e_j \cos E_j)(\cos(\nu_j + \omega_j) \cos \Omega_j - \sin(\nu_j + \omega_j) \sin \Omega_j \cos i_j) \quad (\text{A.2})$$

$$y_{\text{K}, j} = a_j(1 - e_j \cos E_j)(\cos(\nu_j + \omega_j) \sin \Omega_j + \sin(\nu_j + \omega_j) \cos \Omega_j \cos i_j), \quad (\text{A.3})$$

where i_j is the inclination of the orbital plane, ω_j is the longitude of the pericenter, Ω_j is the position angle of the line of nodes, e_j is the eccentricity, a_j is the apparent semi-major axis of the star's orbit around the system barycenter, i.e. the *astrometric signature*. For what concerns E_j , the eccentric anomaly, is the solution to Kepler's Equation:

$$E_j - e_j \sin E_j = M_j, \quad (\text{A.4})$$

with the mean anomaly M_j , expressed in terms of the orbital period P_j and the epoch of the pericenter passage τ_j :

$$M_j = \frac{2\pi}{P_j}(t - \tau_j) \quad (\text{A.5})$$

Finally, the true anomaly ν_j is a function of the eccentricity and the eccentric anomaly:

$$\nu_j = 2 \arctan \left\{ \left(\frac{1 + e_j}{1 - e_j} \right)^{1/2} \tan E_j / 2 \right\} \quad (\text{A.6})$$

We then rotate on the ecliptic reference frame by means of the transformation matrix:

$$\mathbf{R}(\lambda_b, \beta_b) = \begin{pmatrix} -\sin \lambda_b & -\sin \beta_b \cos \lambda_b & \cos \beta_b \cos \lambda_b \\ \cos \lambda_b & -\sin \beta_b \sin \lambda_b & \cos \beta_b \sin \lambda_b \\ 0 & \cos \beta_b & \sin \beta_b \end{pmatrix}$$

The other two vectors in Eq. A.1 are thus defined as:

$$\begin{aligned} \mathbf{x}_{\text{ecl}}^{\text{K}, j} &= \mathbf{R}(\lambda_b, \beta_b) \cdot \mathbf{x}_{\text{K}, j} \\ &= \begin{pmatrix} -\sin \lambda_b \varrho_j \cos \vartheta_j - \sin \beta_b \cos \lambda_b \varrho_j \sin \vartheta_j \\ \cos \lambda_b \varrho_j \cos \vartheta_j - \sin \beta_b \sin \lambda_b \varrho_j \sin \vartheta_j \\ \cos \beta_b \varrho_j \sin \vartheta_j \end{pmatrix} \end{aligned}$$

$$\begin{aligned}\mathbf{x}_{\text{ecl}}^{\pi,\mu} &= \mathbf{R}(\lambda_b, \beta_b) \cdot \mathbf{x}_{\pi,\mu} \\ &= \begin{pmatrix} -\sin \lambda_b \{\mu_\lambda t + \pi F_\lambda\} - \sin \beta_b \cos \lambda_b \{\mu_\beta t + \pi F_\beta\} \\ \cos \lambda_b \{\mu_\lambda t + \pi F_\lambda\} - \sin \beta_b \sin \lambda_b \{\mu_\beta t + \pi F_\beta\} \\ \cos \beta_b \{\mu_\beta t + \pi F_\beta\} \end{pmatrix}\end{aligned}$$

This allows us to write Eq. A.1 in the form:

$$\begin{pmatrix} x_{\text{ecl}} \\ y_{\text{ecl}} \\ z_{\text{ecl}} \end{pmatrix} = \begin{pmatrix} \cos \beta_b \cos \lambda_b - \sin \lambda_b \varrho_j \cos \vartheta_j - \sin \beta_b \cos \lambda_b \sum_{j=1}^{n_p} \varrho_j \sin \vartheta_j \\ -\sin \lambda_b \{\mu_\lambda t + \pi F_\lambda\} - \sin \beta_b \cos \lambda_b \{\mu_\beta t + \pi F_\beta\} \\ \cos \beta_b \sin \lambda_b + \cos \lambda_b \sum_{j=1}^{n_p} \varrho_j \cos \vartheta_j - \sin \beta_b \sin \lambda_b \sum_{j=1}^{n_p} \varrho_j \sin \vartheta_j \\ + \cos \lambda_b \{\mu_\lambda t + \pi F_\lambda\} - \sin \beta_b \sin \lambda_b \{\mu_\beta t + \pi F_\beta\} \\ \sin \beta_b + \cos \beta_b \sum_{j=1}^{n_p} \varrho_j \sin \vartheta_j + \cos \beta_b \{\mu_\beta t + \pi F_\beta\} \end{pmatrix}$$

Finally, a rotation to the local reference frame defined by the Instantaneous Great Circles is made by means of the transformation matrix (e.g., ESA 1997):

$$\mathbf{x}_{\text{IGC}} = \mathbf{R}(\lambda_p, \beta_p) \cdot \mathbf{x}_{\text{ecl}}, \quad (\text{A.7})$$

where:

$$\mathbf{R}(\lambda_p, \beta_p) = \begin{pmatrix} -\sin \lambda_p & \cos \lambda_p & 0 \\ -\sin \beta_p \cos \lambda_p & -\sin \beta_p \sin \lambda_p & \cos \beta_p \\ \cos \beta_p \cos \lambda_p & \cos \beta_p \sin \lambda_p & \sin \beta_p \end{pmatrix}$$

and λ_p, β_p are the coordinates of the pole of the IGC at any given time. The resulting vector can be expressed in terms of the two angular coordinates ψ and η :

$$\mathbf{x}_{\text{IGC}} = \begin{pmatrix} x_{\text{IGC}} \\ y_{\text{IGC}} \\ z_{\text{IGC}} \end{pmatrix} = \begin{pmatrix} \cos \psi \cos \eta \\ \cos \eta \sin \psi \\ \sin \eta \end{pmatrix}$$

By now expanding in Taylor Series to first order the IGC cartesian position vector of each target, it is possible to derive a set of linearized equations of condition expressing only the observed abscissa ψ as a function of all astrometric parameters and orbital elements. We formally have:

$$\delta \mathbf{x}_{\text{IGC}} = \sum_{m=1}^n \frac{\partial \mathbf{x}_{\text{IGC}}}{\partial a_m} da_m \quad (\text{A.8})$$

The n unknowns a_m represent positions, proper motions, parallax, and the $7 \star n_p$ orbital elements (if the star is not single). Now consider that:

$$\begin{aligned}\delta \mathbf{x}_{\text{IGC}} &= \delta(x_{\text{IGC}}, y_{\text{IGC}}, z_{\text{IGC}}) = (\delta(\cos \psi \cos \eta), \delta(\sin \psi \cos \eta), \delta \sin \eta) \\ &= (-\sin \psi \cos \eta d\psi - \sin \eta \cos \psi d\eta, \cos \psi \cos \eta d\psi - \sin \eta \sin \psi d\eta, \cos \eta d\eta) \\ &= (-\sin \psi \cos \eta d\psi, \cos \psi \cos \eta d\psi, 0) \\ &\quad + (-\sin \eta \cos \psi d\eta, -\sin \eta \sin \psi d\eta, \cos \eta d\eta) \\ &= \cos \eta (-\sin \psi, \cos \psi, 0) d\psi + (-\sin \eta \cos \psi, -\sin \eta \sin \psi, \cos \eta) d\eta \\ &= \cos \eta d\psi \mathbf{e}_\psi + d\eta \mathbf{e}_\eta\end{aligned}$$

where \mathbf{e}_η and \mathbf{e}_ψ constitute the pair of orthogonal unit vectors in the directions parallel to ψ and η , as defined in the tangent plane. We then have:

$$\cos \eta d\psi \mathbf{e}_\psi + d\eta \mathbf{e}_\eta = \sum_{m=1}^n \frac{\partial \mathbf{x}_{\text{IGC}}}{\partial a_m} da_m \quad (\text{A.9})$$

By taking the scalar product with \mathbf{e}_ψ , we obtain the following scalar expression:

$$\cos \eta d\psi = (-\sin \psi) \sum_{m=1}^n \frac{\partial x_{\text{IGC}}}{\partial a_m} da_m + (\cos \psi) \sum_{m=1}^n \frac{\partial y_{\text{IGC}}}{\partial a_m} da_m \quad (\text{A.10})$$

If we now define:

$$c_{a_m} = (-\sin \psi) \frac{\partial x_{\text{IGC}}}{\partial a_m} + (\cos \psi) \frac{\partial y_{\text{IGC}}}{\partial a_m}, \quad (\text{A.11})$$

then the linearized condition equation takes the form:

$$\cos \eta d\psi = \sum_{m=1}^n c_{a_m} da_m = F(\lambda, \beta, \mu_\lambda, \mu_\beta, \pi, a_j, P_j, \tau_j, \omega_j, \Omega_j, e_j, i_j), \quad j = 1, \dots, n_p \quad (\text{A.12})$$

For each given target, there will be as many equations of this form as the number of observation epochs. The quantity $d\psi = \psi_{\text{obs}} - \psi_{\text{cat}}$ is defined as the difference between the observed and catalog abscissa.